125

Technical Report No. 32-639

The Development of Metal Honeycomb Energy-Absorbing Elements

R. K. McFarland, Jr.

JET PROPULSION LABORATORY
CALIFORNIA INSTITUTE OF TECHNOLOGY
PASADENA, CALIFORNIA

July 24, 1964

Technical Report No. 32-639

The Development of Metal Honeycomb Energy-Absorbing Elements

R. K. McFarland, Jr.

M. E. Alper

M. E. Alper, *Chief*
Applied Mechanics

JET PROPULSION LABORATORY
CALIFORNIA INSTITUTE OF TECHNOLOGY
PASADENA, CALIFORNIA

July 24, 1964

Prepared Under Contract No. NAS 7-100
National Aeronautics & Space Administration

CONTENTS

FIGURES

FIGURES (Cont'd)

FIGURES (Cont'd)

ABSTRACT

The results of an experimental development program to evaluate and optimize metal honeycomb elements for use as axial energy absorbers are presented. The results indicate the potential of metal honeycomb elements for this purpose, and the range of variables to be considered in the design and optimization of these elements.

Author

I. INTRODUCTION

The need for reliable, lightweight, energy-absorbing elements for lunar and planetary vehicle landing systems has resulted in a considerable number of publications. Many techniques have been conceived; a few have been developed to a point where true merit and range of application can be determined.

Restricting the scope of this report to noninflatable energy-absorbing devices (since the inflatable devices such as air bags are systems that bear special consideration), there are two general types or classes of elements to be considered: (1) those that are essentially distributed, such as foams, balsa wood, and honeycomb, and (2) those that are discrete energy absorbers, such as a collapsible or frangible tube or cylinder. (There are, of course, many variations of these two classes. Also, although those techniques classified as distributed could be used in a discrete application, the reverse does not necessarily follow.)

The range of application of these various techniques could be classified in the same manner; a distributed system such as the *Ranger* entry capsule, or a discrete system such as a strut-type shock absorber. In the subject literature (see Bibliography) the proposed techniques can be grouped in a like manner. An additional fact which becomes apparent from a consideration of the literature is that little effort has been made to completely define the parameters involved in the evaluation of an energy-absorbing system or to evaluate more than its most obvious characteristics. In this regard, it is unlikely that one parameter will ever be used as a sole basis for application or evaluation.

The purpose of this report is to present the results of a JPL development effort, to evaluate honeycomb structural elements as energy absorbers and to determine the merits, limitations, and range of applications of this type of energy-absorbing system primarily for application to unmanned lunar or planetary landing vehicles.

II. ENERGY ABSORBERS

If we consider the physical conversion that is brought about by a system that absorbs or dissipates energy, several statements can be made. Assuming that no change in the system potential energy occurs in the process, then the conversion is directly that of transforming kinetic energy to thermal energy. Utilizing this concept, we can define an ideal efficiency for an energy-absorbing system by considering the amount of energy that could be absorbed by a high-heat-capacity material by raising the temperature from ambient to the melting point in an adiabatic process, not including the heat of fusion. For example, with aluminum, theoretical specific energy values of 267 Btu/lb or 208,000 ft-lb/lb could be obtained if the total energy capacity could be utilized in absorbing kinetic energy. Present energy-absorbing systems exhibit specific energies an order of magnitude less than this value. The above-defined efficiency is just one characteristic of an energy-absorbing system; there are several additional characteristics that are equally pertinent. For example, the variation of load during deformation (i.e., the deceleration-time response) is a characteristic that will indicate another type of efficiency. The more constant the load during the deformation (or the deceleration force during the impact period) the more efficient the system. In addition, the less energy stored, as indicated by minimum rebound, the more efficient the

system. These last two system characteristics are often referred to by stating that a system has a "rectangular force response."

Static load tests of energy-absorbing systems, where axial load is applied at a rate of the order of 1–10 in./min, provide an indication of the characteristic response of an energy-absorbing system to an axial load, particularly with regard to determining how rectangular the force response is, which would include a measure of the elastic response or rebound. For most systems it has been established that there is good correlation between quasistatic and dynamic energy absorption when the impact velocity of the dynamic load is limited to something less than 50 ft/sec. This latter relationship must be established for each material or system considered, and at present little experimental information exists with which to establish the extension of this correlation for impact velocities in excess of approximately 50 ft/sec.

Other characteristics that contribute to the now equivocal "efficiency" of an energy-absorbing system but which are not considered in this report are the response to a nonaxial load, the ability of the system or element to operate in a deep space environment, and strain rate effects.

III. DEVELOPMENT PROGRAM

A development program was undertaken to determine the optimum specific energy capacity of a honeycomb element, subject to axial loading. Previous efforts at JPL have established a semi-empirical method for determining the mean crushing stress of a hexagonal cell honeycomb (Refs. 1 and 2). It was found that this crushing stress was controlled by the yield stress of the material, both in bending and in shear and the unit weight of the honeycomb. Thus the higher the yield stress and greater the unit weight, the higher the crushing stress.

In addition to the axial crushing stress for an energy-absorbing element, two other quantities must be known to convert to specific energy: namely, the unit weight of the energy-absorbing element and a quantity referred to as the "thickness efficiency." This latter quantity represents the depth to which an element can be crushed; quantitatively, it is the ratio of the stroke length of a fully crushed energy-absorbing element to the original length of the element. Thus:

$$\text{Specific energy} = \frac{(\text{Mean crushing stress}) \times (\text{Thickness efficiency})}{\text{Unit weight}}$$

The means for optimizing these factors were determined by considering and experimentally evaluating the dependent variables involved: namely, the cross-sectional geometry of the honeycomb, the unit weight of the honeycomb, and the yield-strength-to-unit-weight ratio of the material used. Since these factors are mutually dependent, a determination was first made with regard to the cross-sectional geometries to be considered. Several cross-sectional shapes were fabricated from a standard honeycomb material in unit weights indicative of the maximum range feasible.

Static and dynamic tests were then performed on the specimens in order to evaluate the mutual effect of cross-sectional geometry on crushing stress, unit weight, and thickness efficiency—all dependent variables. A final evaluation was performed using a material exhibiting a very large ratio of yield stress to density ratio and a standard hexagonal cell geometry, thus experimentally

establishing a quantitative relationship between all the primary variables that affect the energy-absorbing capacity of a honeycomb element for axial loading.

A. Geometry

For the evaluation of the effect of changing cross-sectional geometry, in addition to the basic hexagonal cell honeycomb (Fig. 1), three cross-sections were considered: a close-pack array of cylinders, a loose-pack array of cylinders, and a modified hexagonal cell shape (see Figs. 2-4). As shown in Fig. 4, the cross-sectional of the modified hexagonal cell shape proved to be completely unsatisfactory owing to the large difference in cross-sectional strength, and no further mention will be made of it.

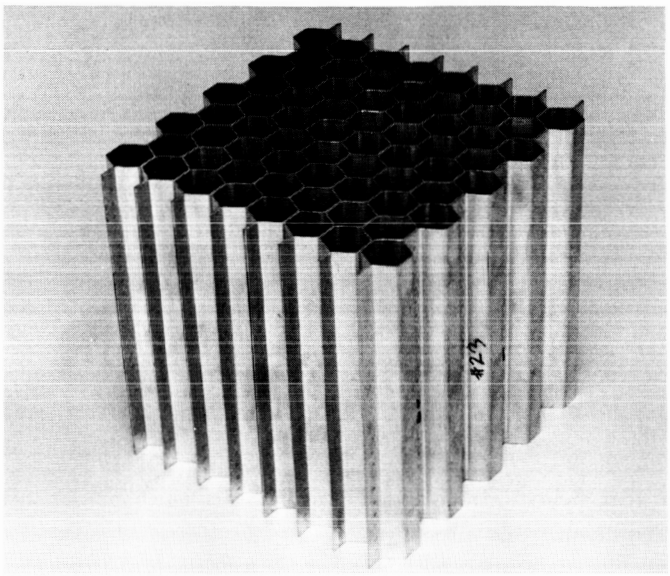

Fig. 1. Typical hexagonal cell honeycomb specimen

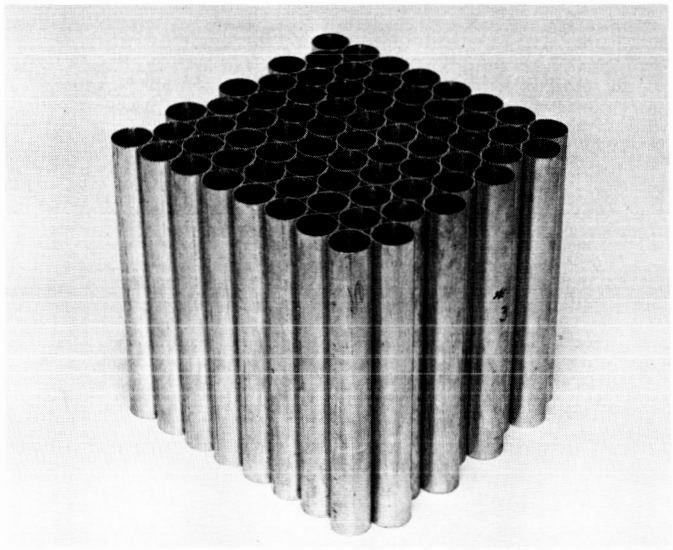

Fig. 2. Typical close-pack tubular cell honeycomb specimen

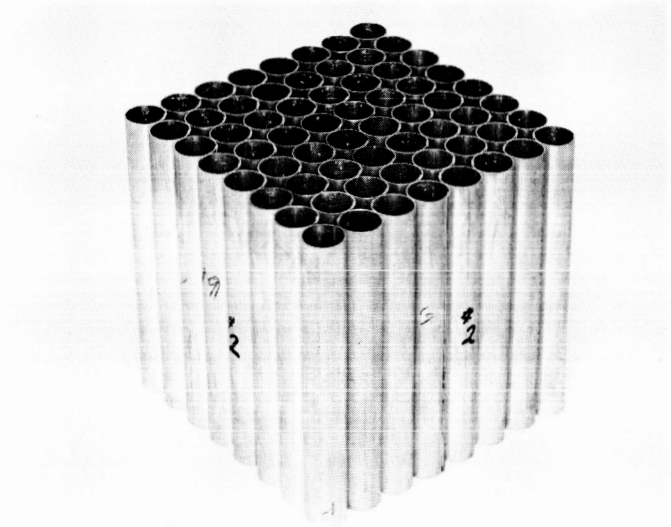

Fig. 3. Typical loose-pack tubular cell honeycomb specimen

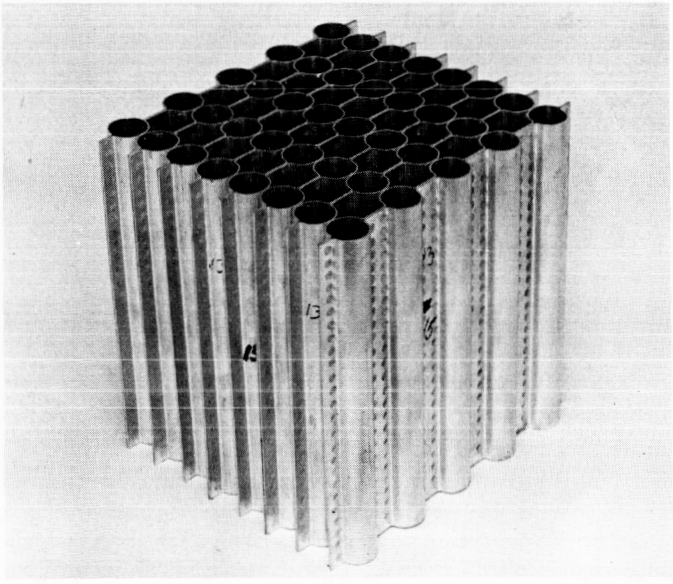

Fig. 4. Typical modified hexagonal cell honeycomb specimen

B. Honeycomb Unit Weight

To evaluate the cross-sectional geometries considered, a number of specimens were fabricated for each geometry in several unit weights. Now, since primary interest was in the hexagonal cell honeycomb, an alloy commonly used in commercial honeycomb (3003 H-19 aluminum) was used in fabricating all specimens to allow correlation with available test data. The specimens were fabricated in unit weights exceeding those commercially available, the purpose being to determine the effect of unit weight change on the specific energy and the limiting unit weight for each geometry considered. All specimens were fabricated with a ¾-in. cell (or tube) diameter and with a wall thickness adjusted to give the desired unit weight. The cell arrays were assembled using spot-welding techniques rather than adhesive bonding, since experiments had shown that bonding does not provide adequate structural integrity for the higher unit weight

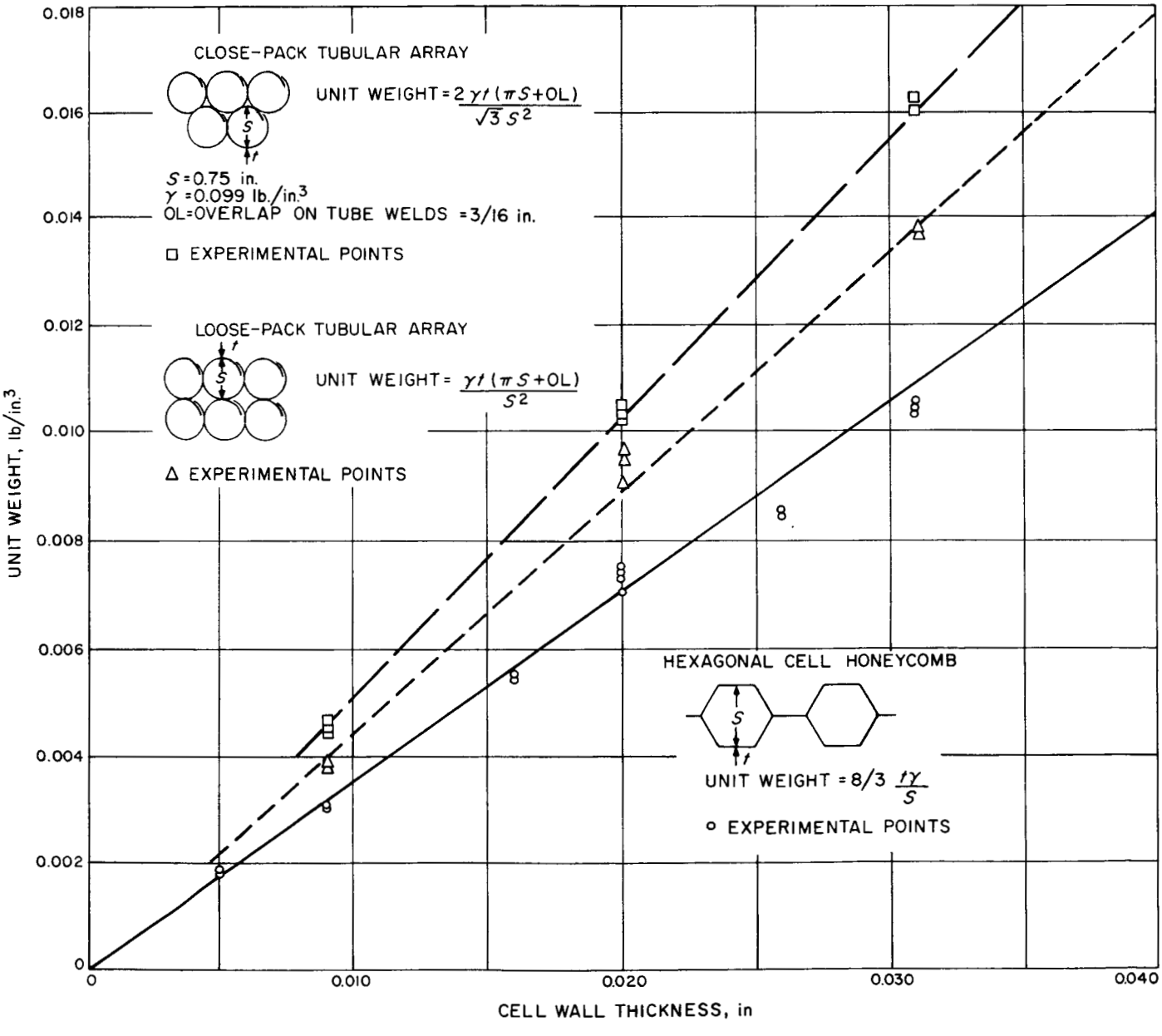

Fig. 5. Honeycomb unit weight, 3003 H-19 aluminum

arrays. All honeycomb elements were fabricated in rectangular arrays measuring approximately 6 in. on a side.

The hexagonal cell honeycomb was fabricated in six unit weights by using cell wall thicknesses of 0.005, 0.009, 0.016, 0.020, 0.026, and 0.031 in. The two tubular array geometries were fabricated in only three unit weights utilizing cell wall thicknesses of 0.009, 0.020, and 0.031 in. Since the tubular arrays are essentially a modification of the hexagonal cell geometry, a fewer number of unit weights were selected to establish the effect of the geometry change. Figure 5 shows the unit weights of the specimens for computed and measured values.

C. *Testing Program*

Using a standard hydraulic testing machine, axial static tests were performed on the specimens at a loading rate of 1–2 in./min. No effort was made to record the peak buckling, as only the postbuckling response of the honeycomb was of interest. In each of the three cross-sectional geometries, two specimens were tested for each honeycomb unit weight. One test on each unit weight was continued until the specimen was fully collapsed in order to determine thickness efficiencies. Figures 6 through 8 are representative curves of static load vs deformation for each specimen type tested.

A dynamic test was performed on each honeycomb unit weight. This test consisted of dropping a mass on

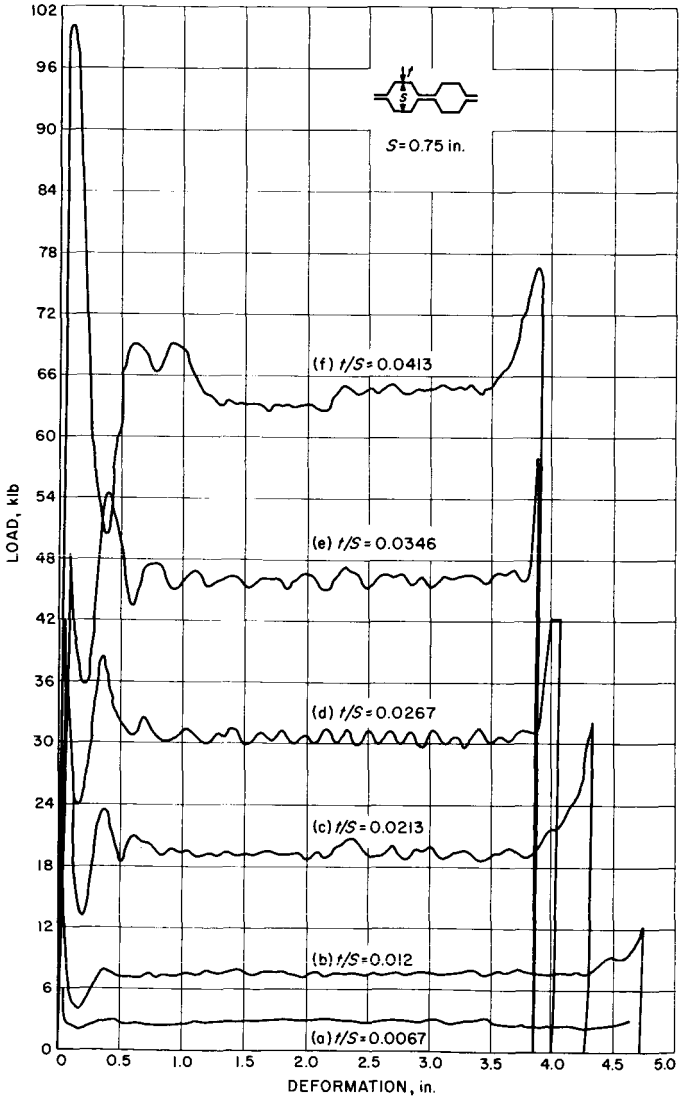

Fig. 6. Static-load deformation curve, hexagonal cell honeycomb, 3003 H-19 aluminum

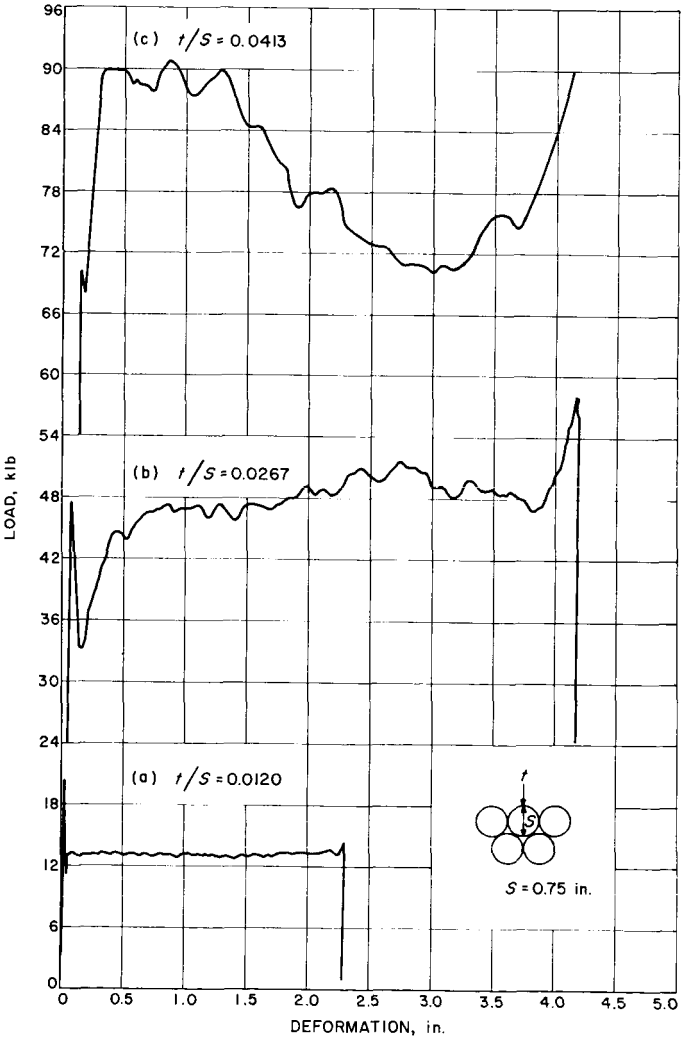

Fig. 7. Static-load deformation curve, close-pack tubular cell honeycomb, 3003 H-19 aluminum

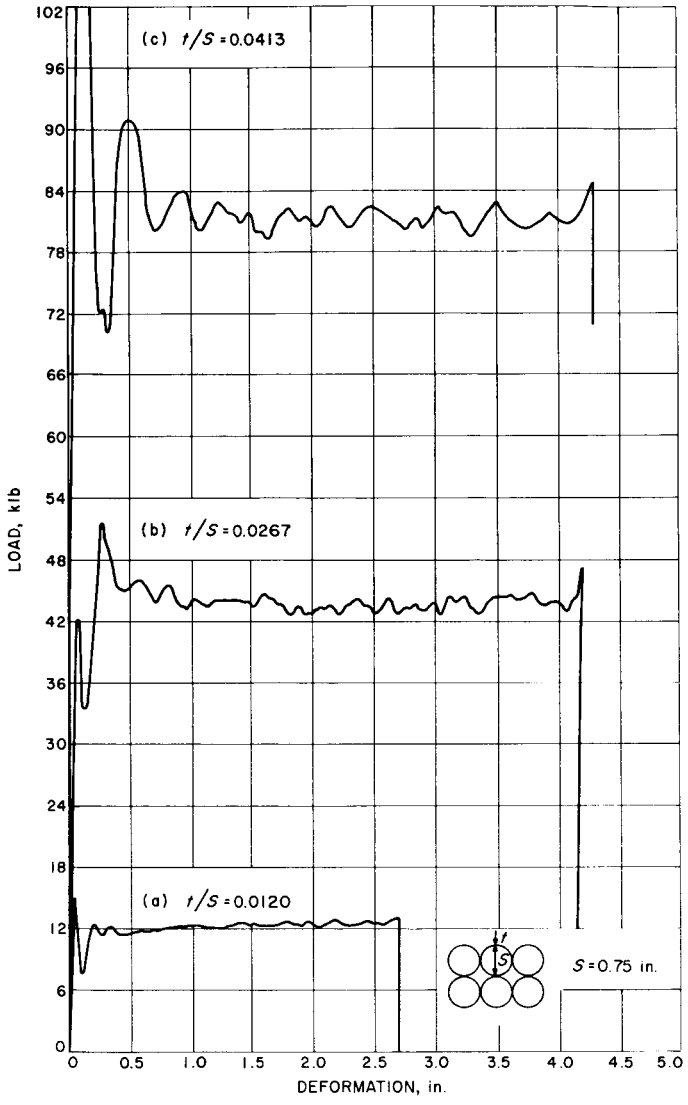

Fig. 8. Static-load deformation curve, loose-pack tubular cell honeycomb, 3003 H-19 aluminum

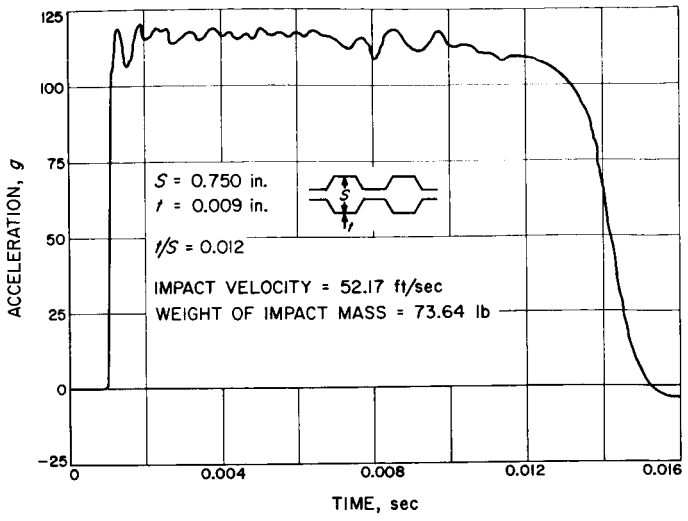

Fig. 9. Acceleration–time response, hexagonal cell honeycomb, 3003 H-19 aluminum

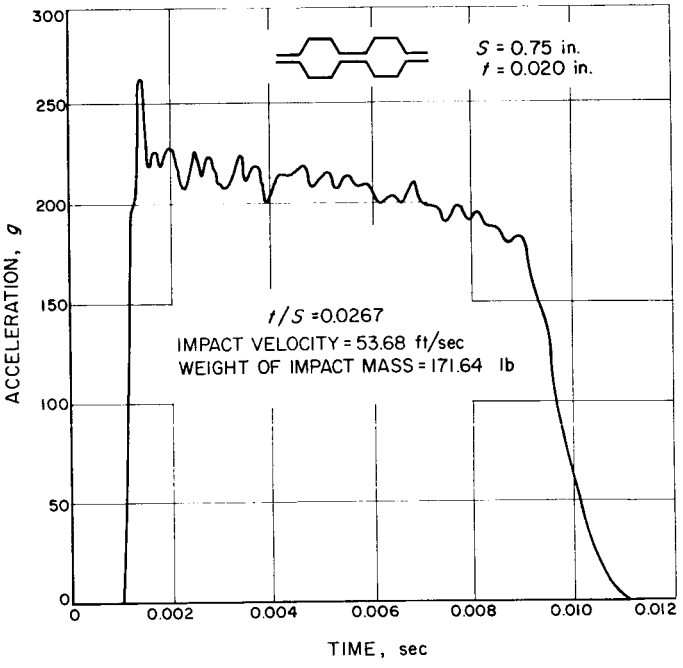

Fig. 10. Acceleration–time response, hexagonal cell honeycomb, 3003 H-19 aluminum

the honeycomb at a given impact velocity, and recording the acceleration vs time response of the impacting mass. The impact velocity was approximately the same for all tests, and the size of the impacting mass was varied so that the specimen to be tested never collapsed more than approximately one-fourth of its length. In this way it was possible to neglect the effect of compressed air trapped inside the honeycomb during the impact. The acceleration transducer was a standard piezoelectric type, used in conjunction with a cathode follower, an amplifier, a 2000-cps filter, and an oscilloscope. The oscilloscope trace of the acceleration vs time response was recorded with a Polaroid camera. Figures 9 through 17 present traces of typical plots of acceleration vs time for all unit weights. Figures 18 through 25 are photographs of typical specimens tested, showing the characteristic mode of response for each cross-sectional geometry tested.

D. Material with High Ratio of Yield Strength to Density

A preliminary survey was conducted and it was found that maraging steel possessed a very good ratio of yield

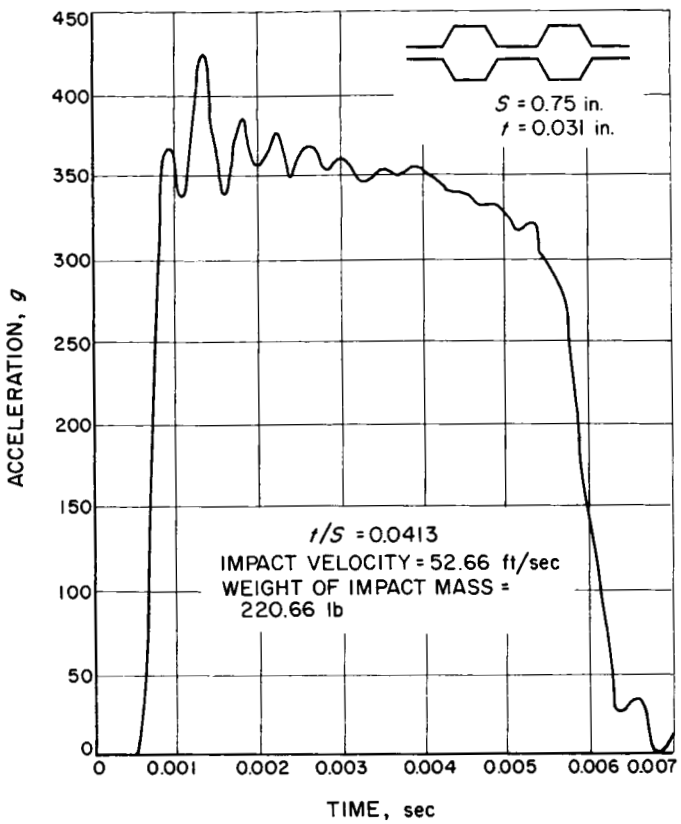

Fig. 11. Acceleration–time response, hexagonal cell honeycomb, 3003 H-19 aluminum

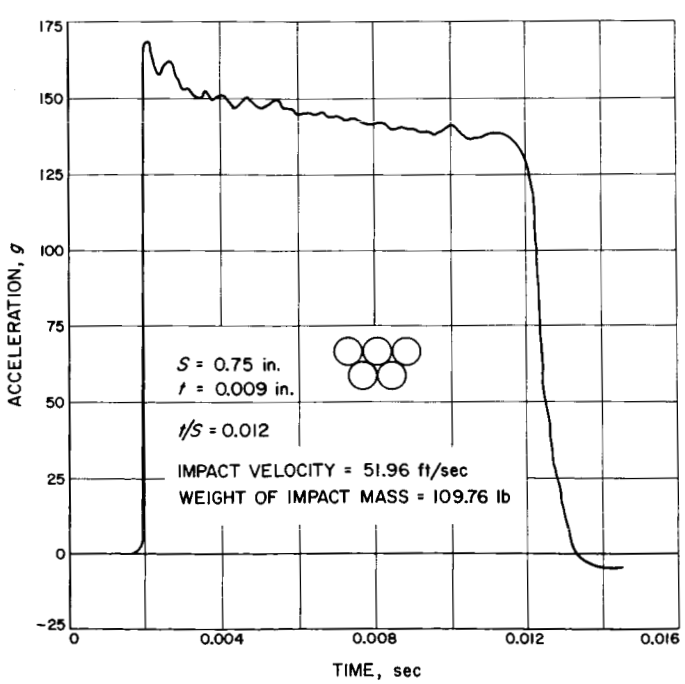

Fig. 12. Acceleration–time response, close-pack tubular cell honeycomb, 3003 H-19 aluminum

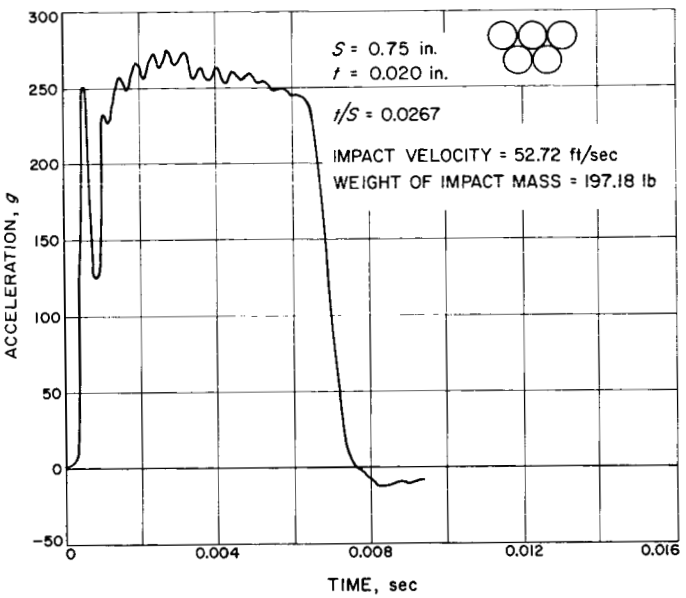

Fig. 13. Acceleration–time response, close-pack tubular cell honeycomb, 3003 H-19 aluminum

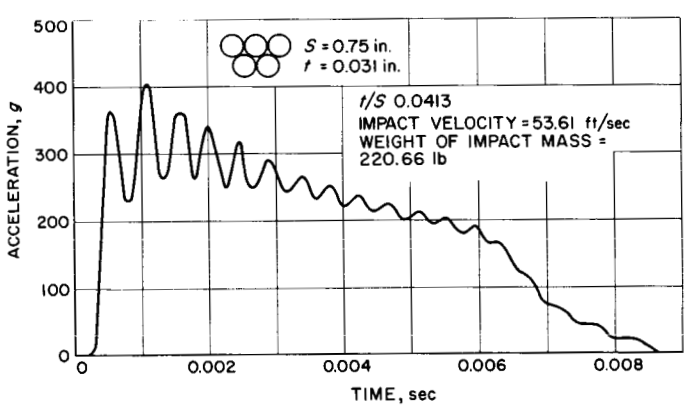

Fig. 14. Acceleration–time response, close-pack tubular cell honeycomb, 3003 H-19 aluminum

stress to density and sufficient ductility to allow it to respond in a typical honeycomb collapsing mechanism. Hexagonal cell specimens were fabricated from maraging steel using the same dimensions as used on the aluminum honeycomb, in three unit weights, with wall thicknesses of 0.008, 0.016, and 0.024 in. The alloy used for the 0.008- and 0.016-in.-wall-thickness specimens was an A-L 25 Ni(250) maraging steel, and the 0.024-in.-wall-thickness specimen was fabricated from an A-L 25 Ni(300) maraging steel; both were obtained from the Allegheny Ludlum Steel Corporation.

Static axial tests were performed on the maraged steel specimen in a manner identical to that employed with

the aluminum alloy specimens. Typical load–deformation curves are shown in Figures 26, 27, and 28.

A dynamic load test was performed only on the low-unit-weight specimen, as the capacity of the available drop tower was approximately 7800 ft-lb, which is too small an energy input to induce the two heavier-density honeycombs to respond. Figure 29 is the acceleration–time trace of this test. Characteristic modes of response of the maraging specimen to static loading are shown in Figures 30 through 33.

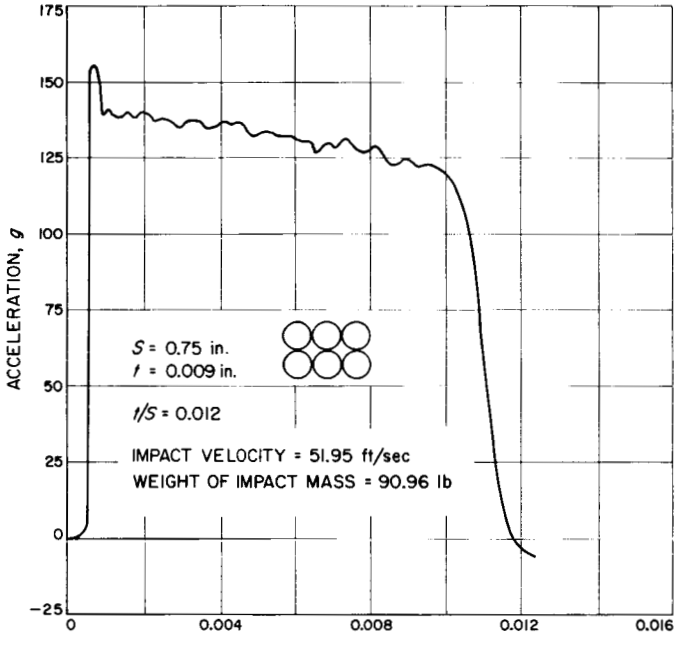

Fig. 15. Acceleration–time response, loose-pack tubular cell honeycomb, 3003 H-19 aluminum

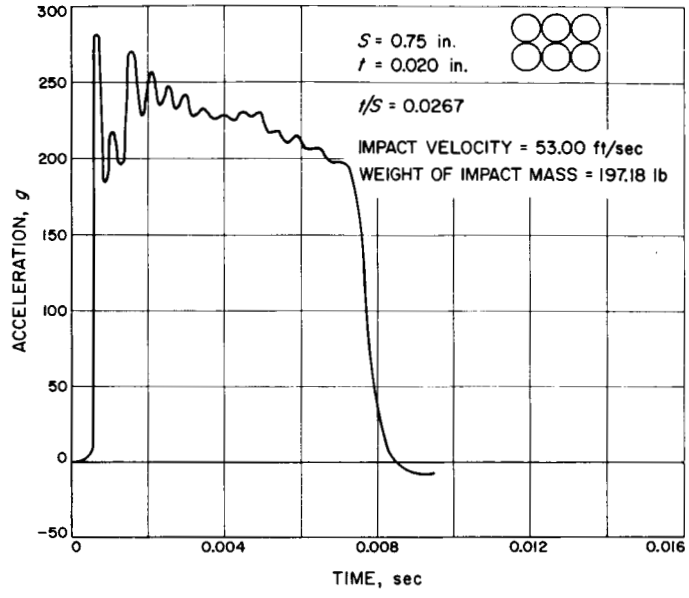

Fig. 16. Acceleration–time response, loose-pack tubular cell honeycomb, 3003 H-19 aluminum

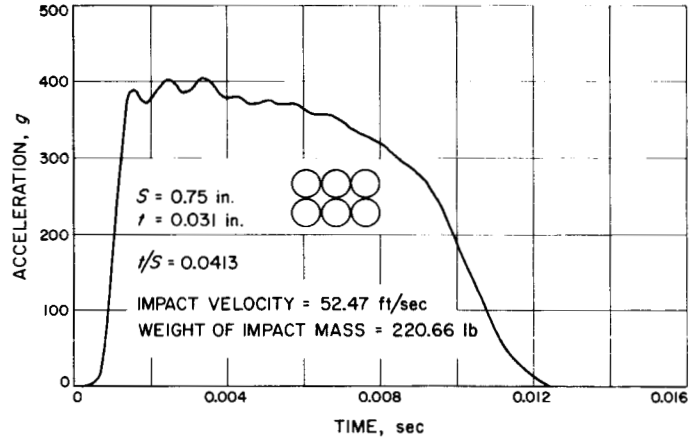

Fig. 17. Acceleration–time response, loose-pack tubular cell honeycomb, 3003 H-19 aluminum

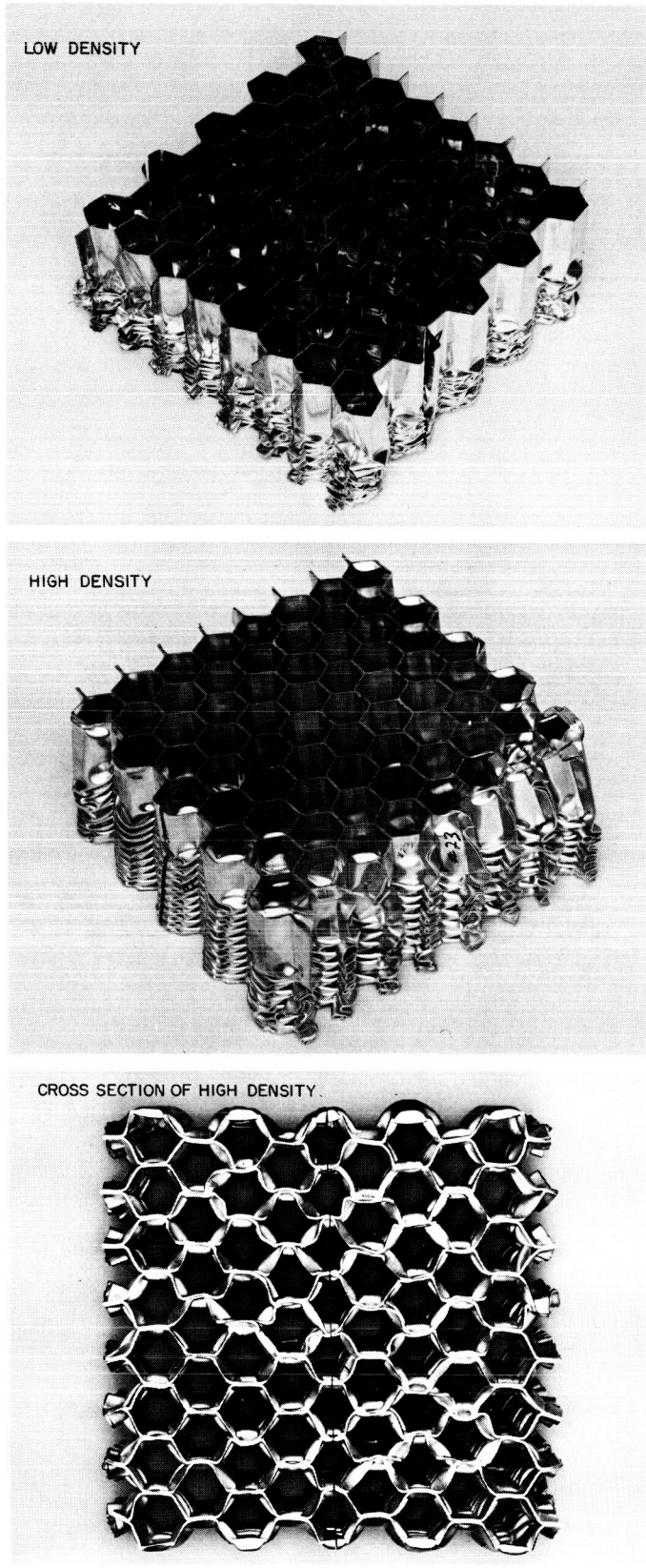

Fig. 18. Hexagonal cell honeycomb

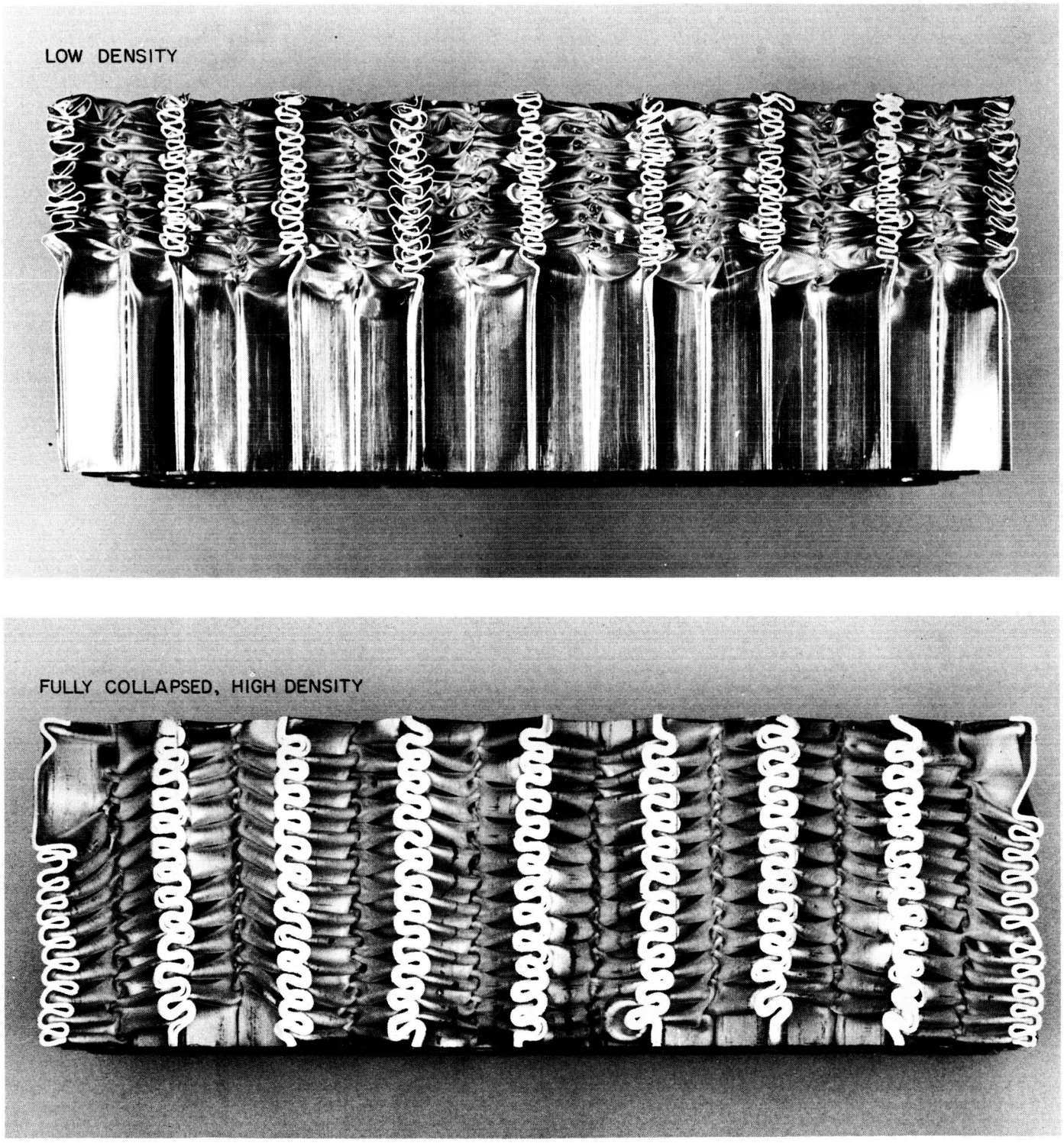

Fig. 19. Cross section of hexagonal cell honeycomb

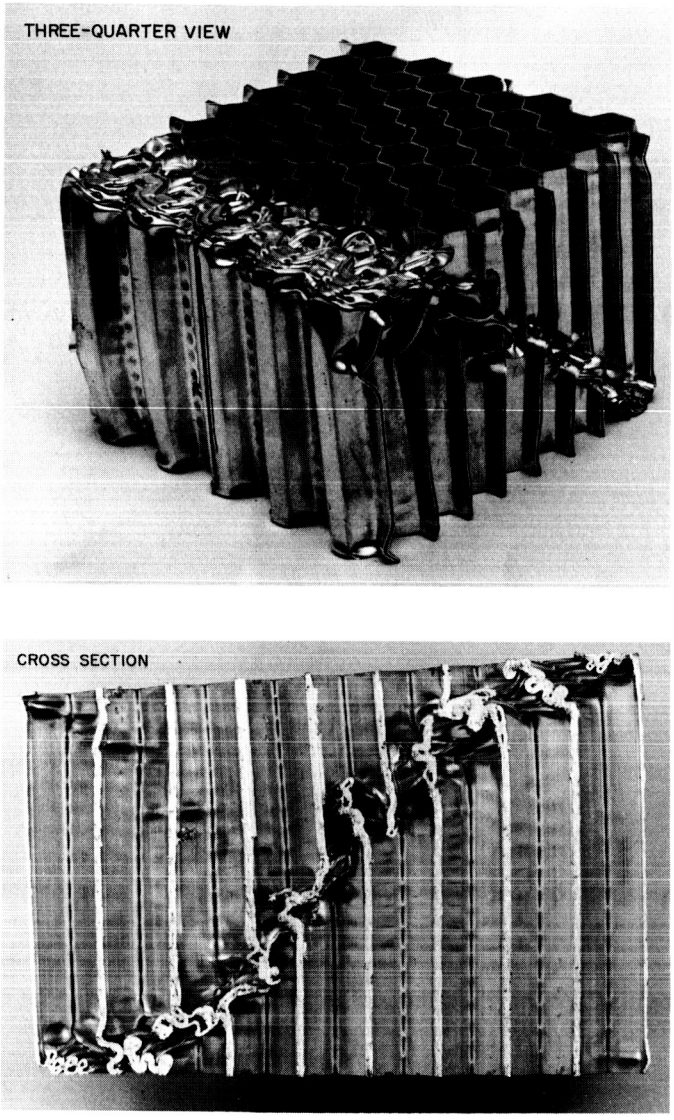

Fig. 20. Shear mode collapse of hexagonal cell honeycomb

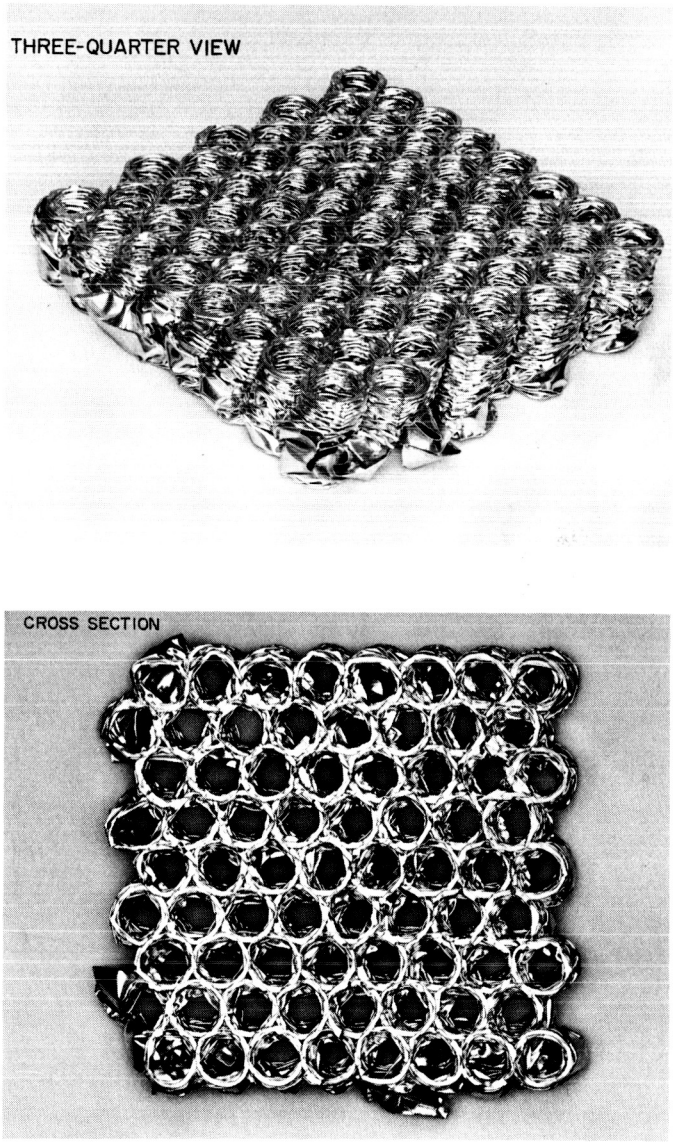

Fig. 21. Close-pack tubular cell honeycomb, fully collapsed

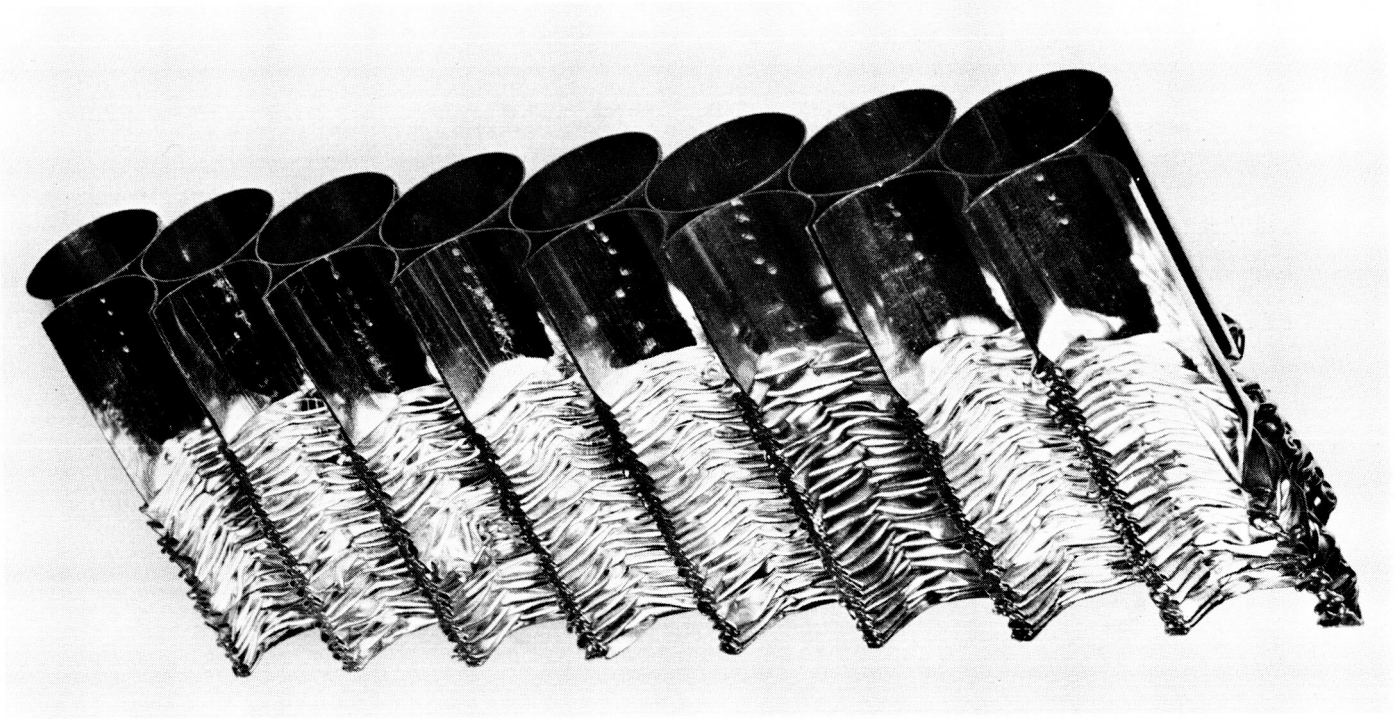

Fig. 22. Cross section of low-unit-weight, close-pack tubular array honeycomb

Fig. 23. High-unit-weight, close-pack tubular array honeycomb, fully collapsed; wall thickness, 0.031 in.

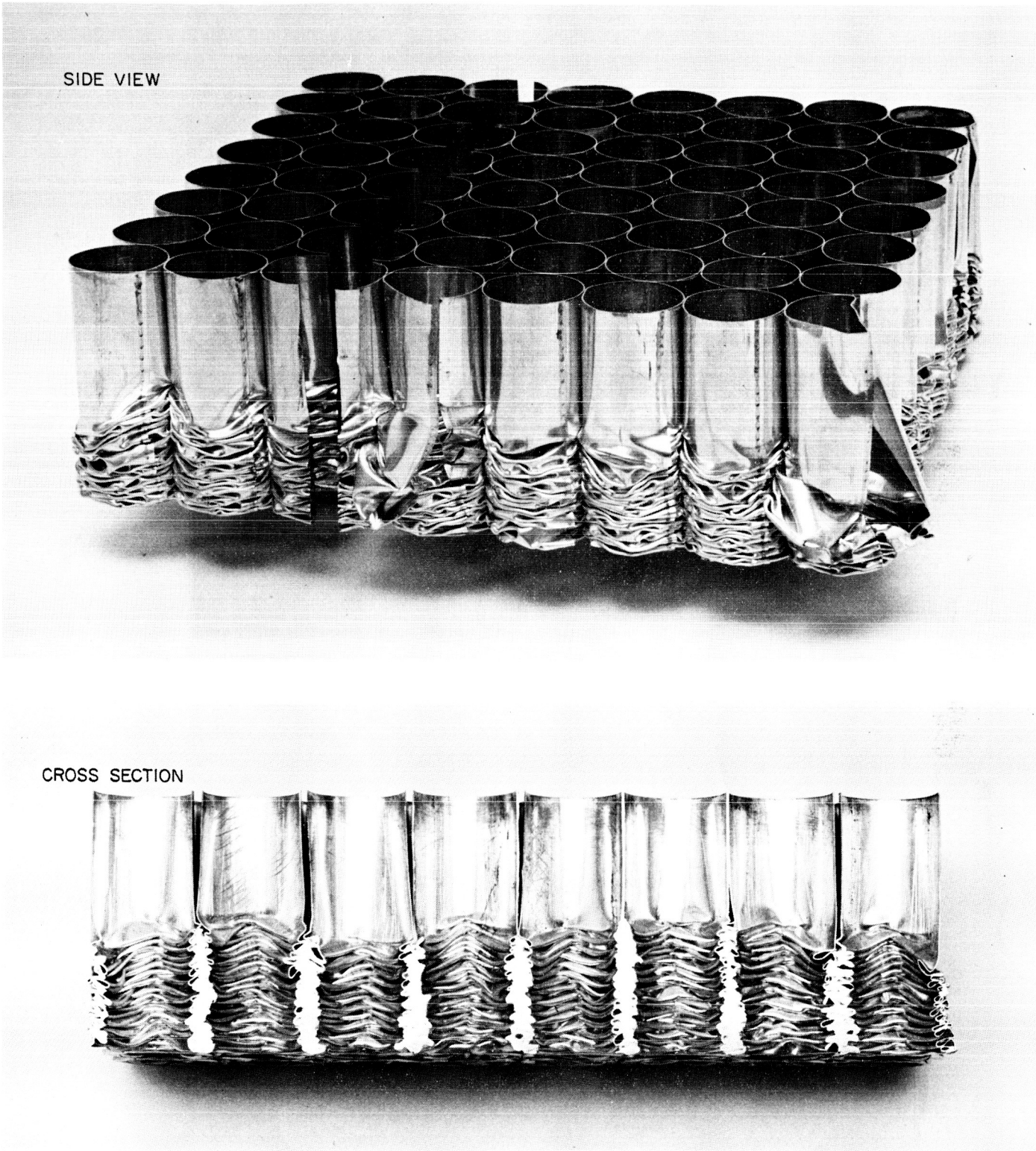

Fig. 24. Low-unit-weight, loose-pack tubular cell honeycomb, partially collapsed; wall thickness, 0.009 in.

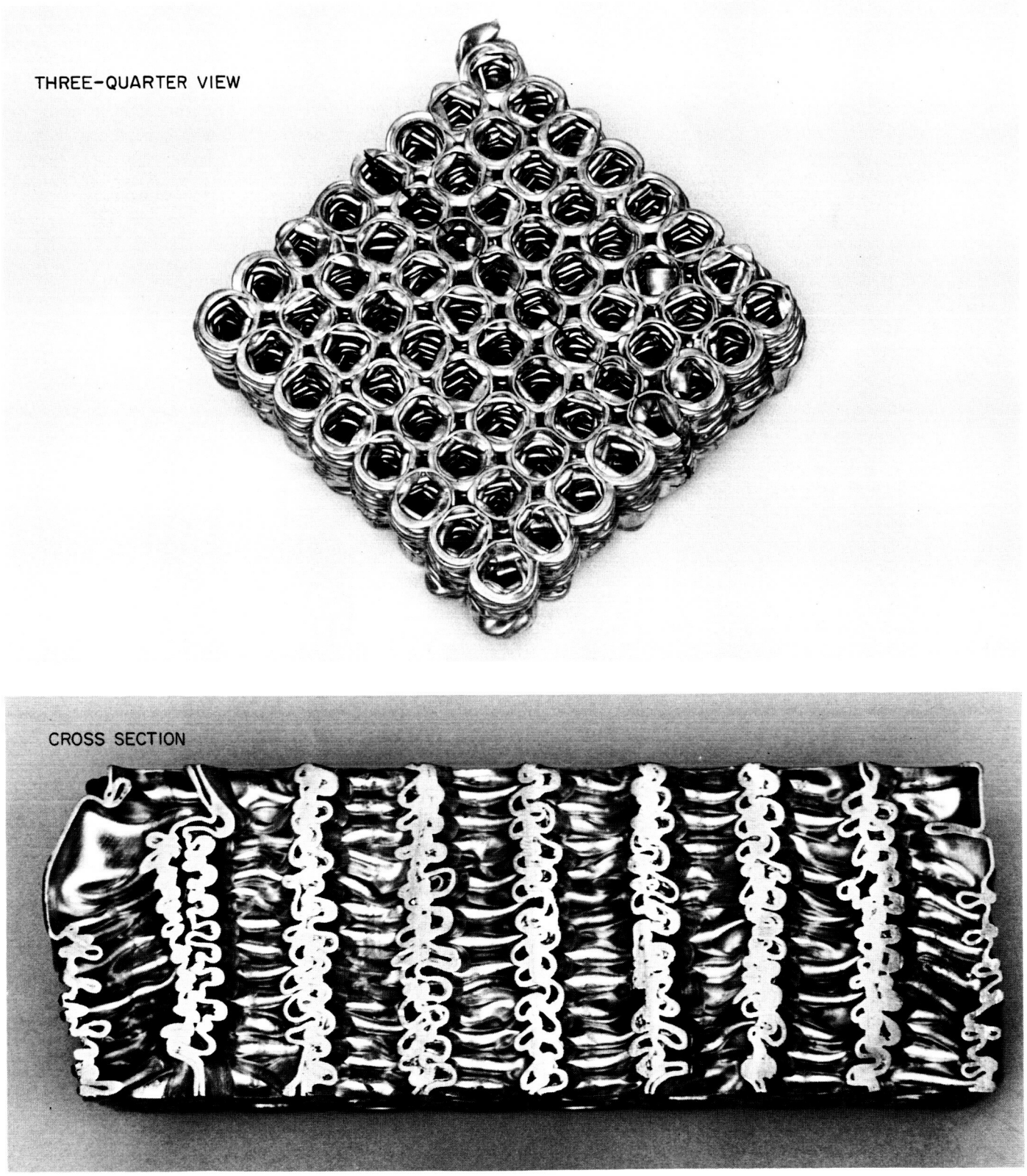

Fig. 25. High-unit-weight, loose-pack tubular cell honeycomb, fully collapsed; wall thickness, 0.031 in.

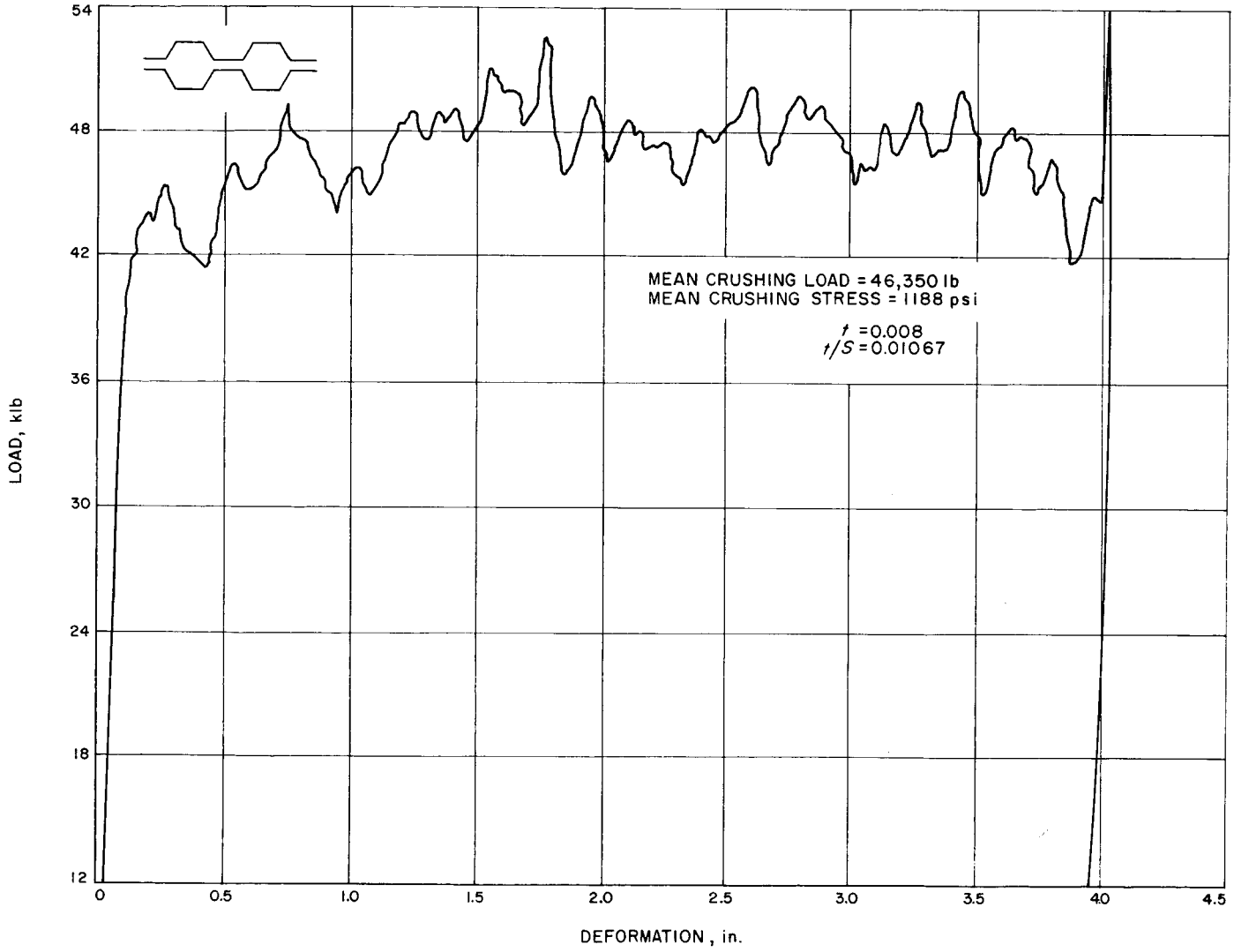

Fig. 26. Static-load deformation curve, maraging steel hexagonal cell honeycomb

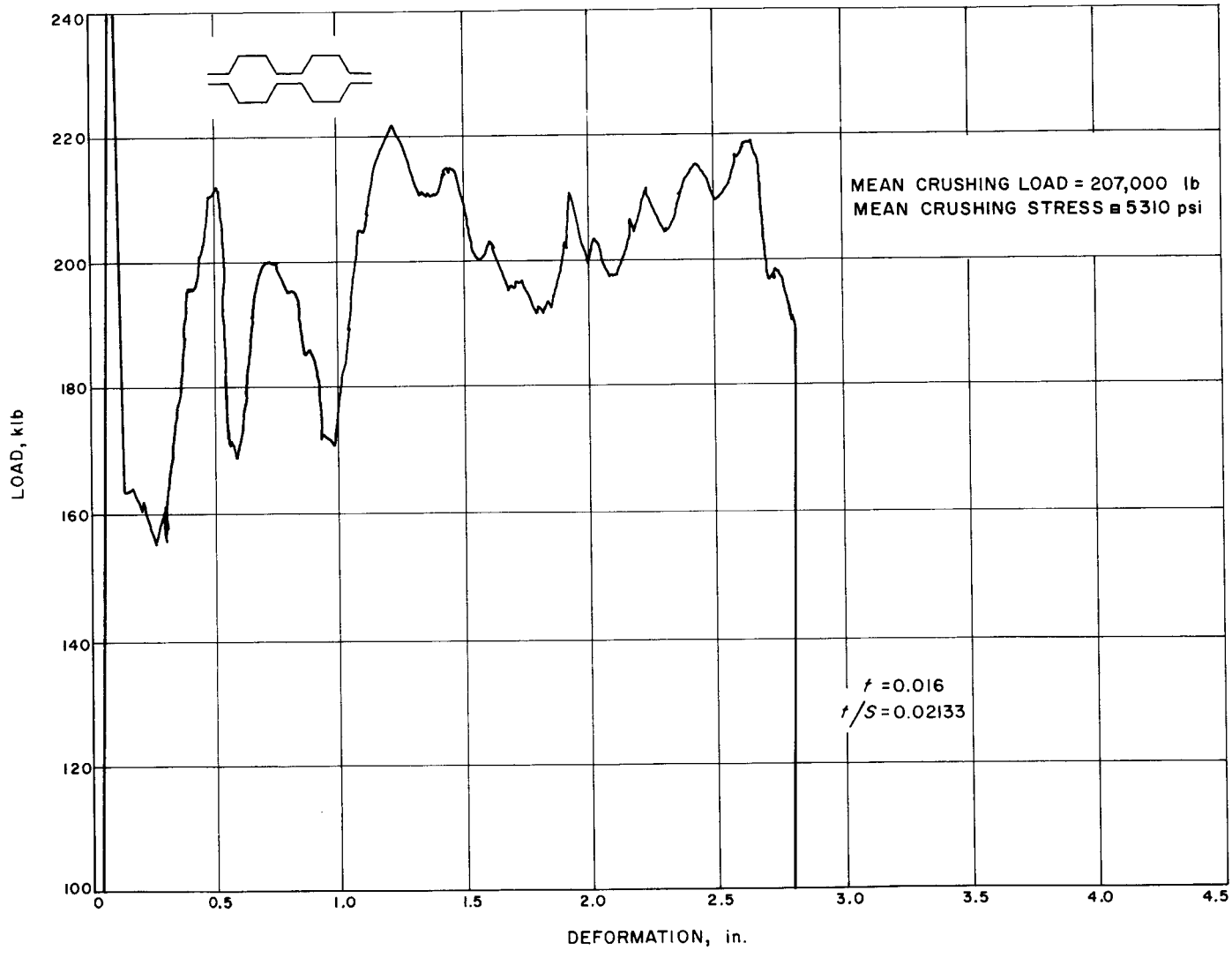

Fig. 27. Static-load deformation curve, maraging steel hexagonal cell honeycomb

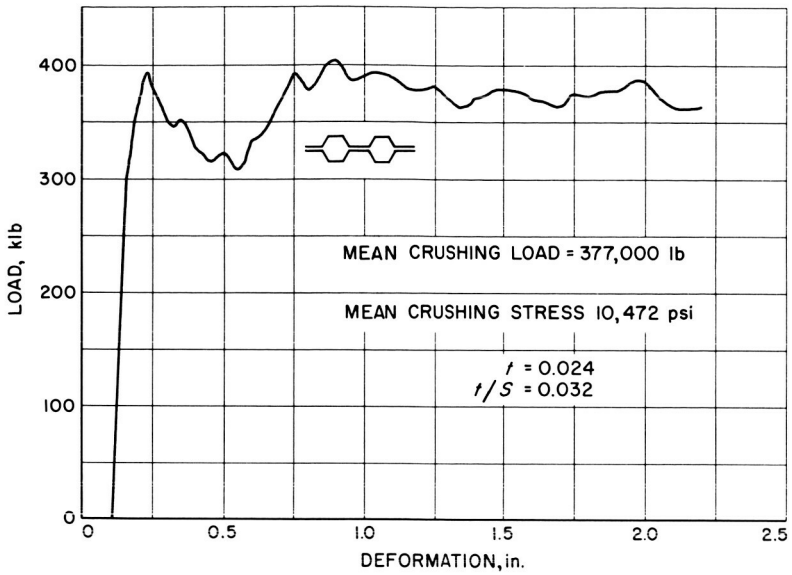

Fig. 28. Static-load deformation curve, maraging steel hexagonal cell honeycomb

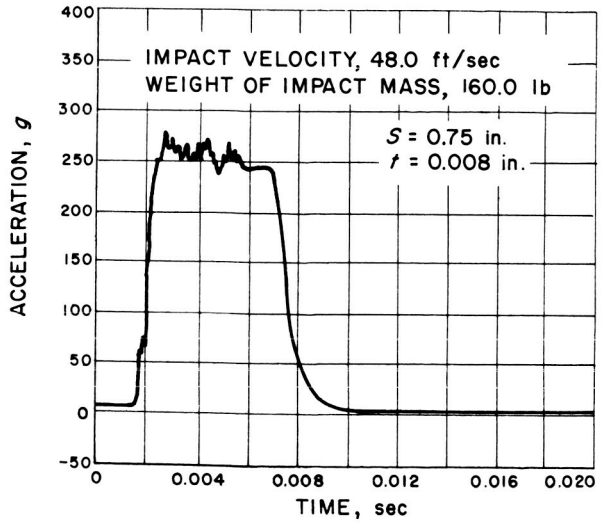

Fig. 29. Dynamic test, maraging steel hexagonal cell honeycomb

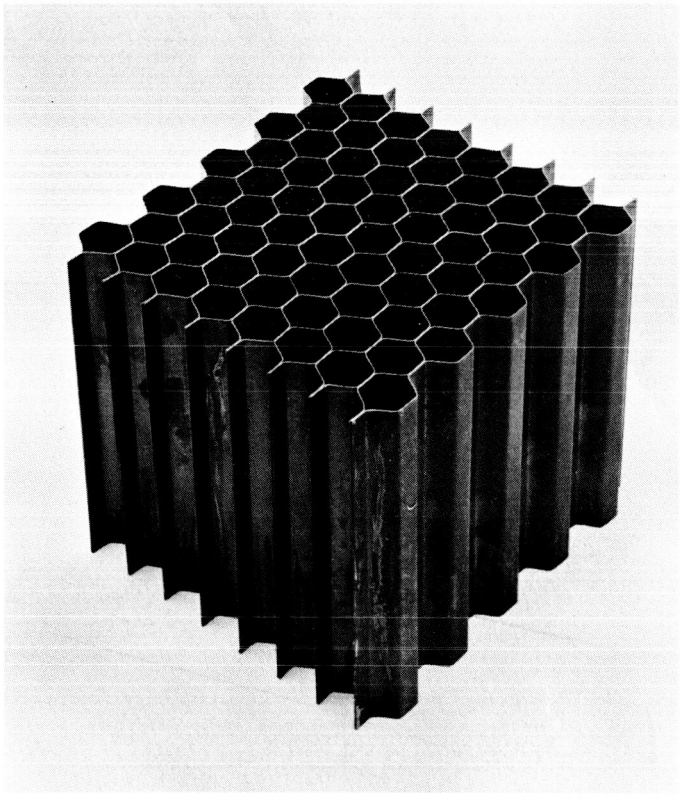

Fig. 30. Typical maraging steel hexagonal cell honeycomb, before testing

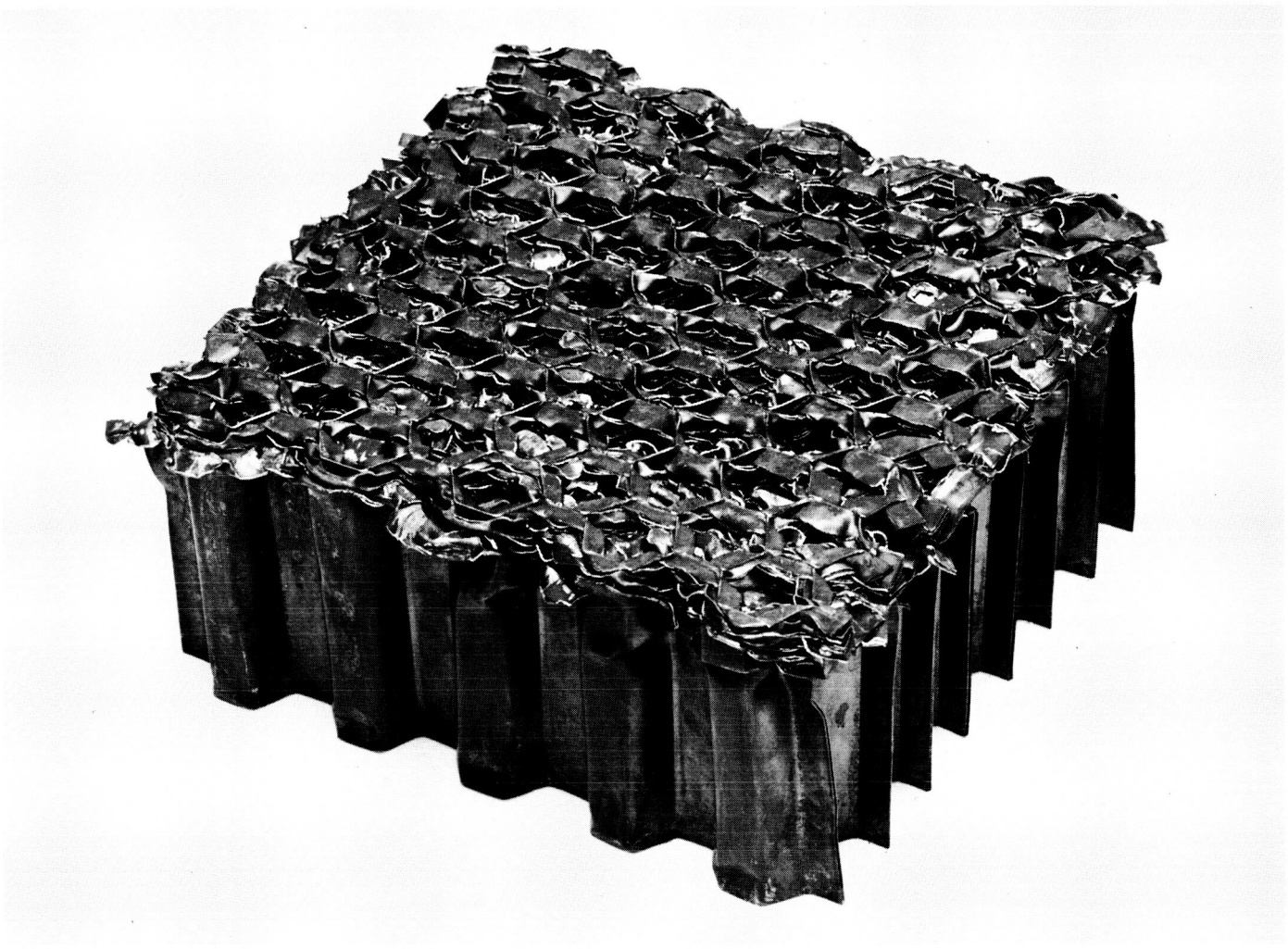

Fig. 31. Partially collapsed maraging steel hexagonal cell honeycomb, wall thickness, 0.016 in.

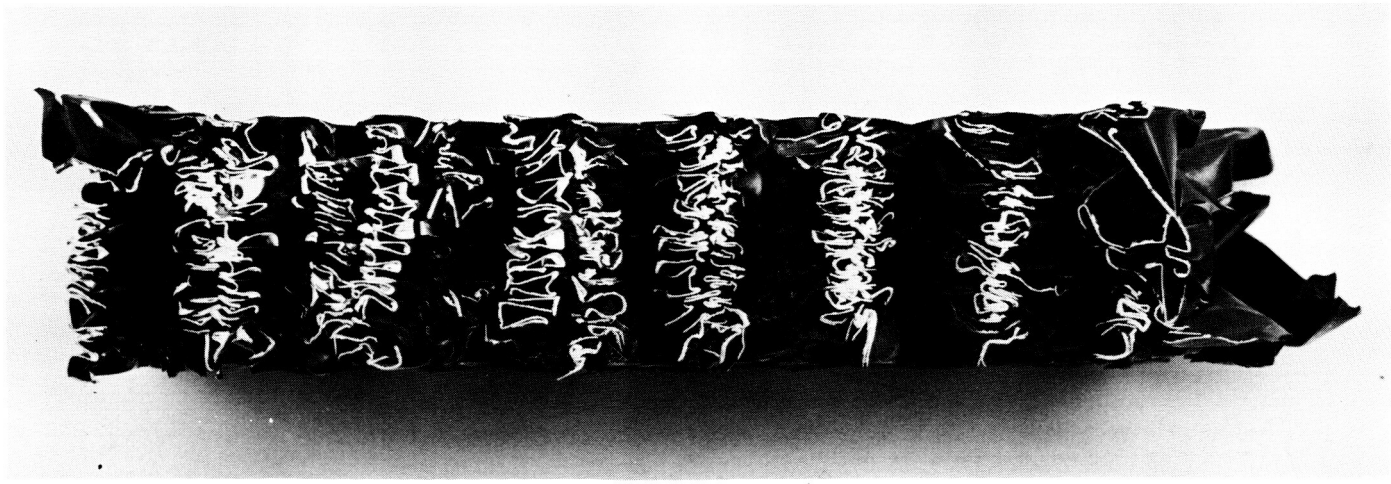

Fig. 32. Cross section of maraging steel hexagonal cell honeycomb, wall thickness, 0.008 in.

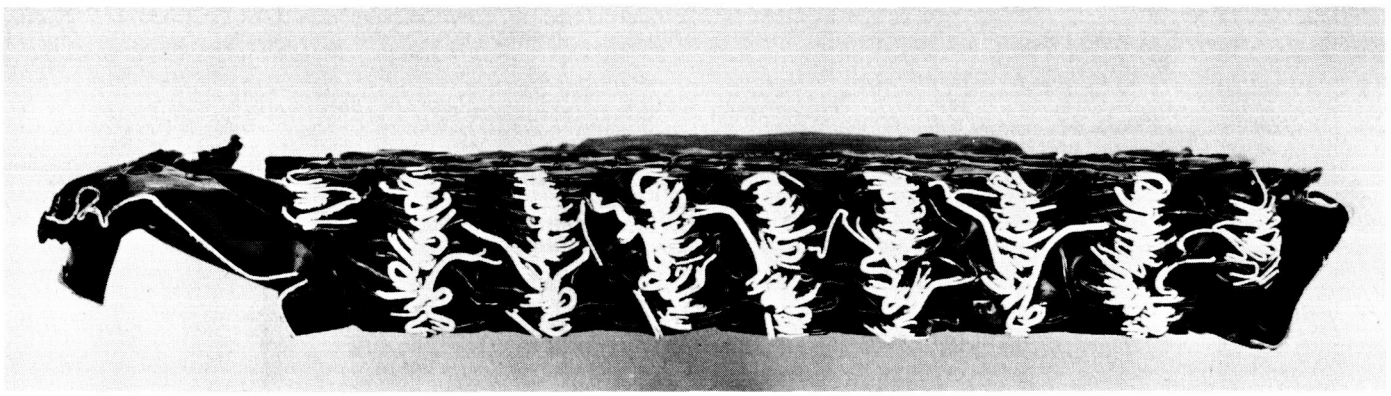

Fig. 33. Cross section of maraging steel hexagonal cell honeycomb, fully collapsed; wall thickness, 0.024 in.

IV. SUMMARY OF RESULTS

A. Geometry

Considering the effect of cross-sectional geometry on the total specific energy of honeycomb, test results indicate that a sizable increase in specific energy can be obtained by using a tubular cell honeycomb rather than the hexagonal cell honeycomb.

Referring to Figure 34, a plot of specific energy values obtained for the three cross-sectional geometries considered for static loading, the tubular cell honeycombs are able to develop specific energies approximately 20% greater than the hexagonal cell honeycomb for the same unit weight. Since a semi-empirical relationship has been established for determining the specific energy of hexagonal cell honeycombs, then this approximate relationship between geometries will provide means of calculating specific energies of tubular cell honeycombs.

The dynamic tests indicated essentially identical results as stated above. However, an additional relationship was established, that of a dependency of specific energy on velocity of impact. For an impact velocity of approximately 50 ft/sec used in all dynamic tests, there was a small increase in specific energy for dynamic loading as compared to static loading for all specimens tested. This relationship is shown in Fig. 35.

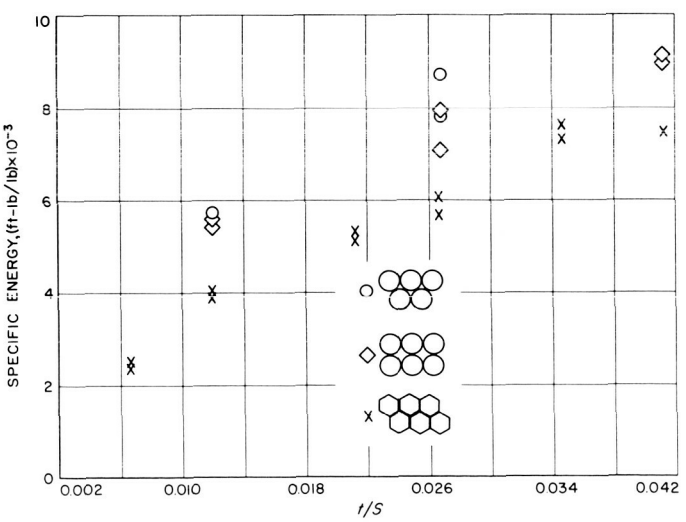

Fig. 34. Static-loading specific energy, 3003 H-19 aluminum

Also, it was found that the dynamic tests provided means of critically evaluating the structural integrity of the honeycomb elements. Several specimens failed because of poor spot welding during dynamic tests, although the same specimens had been effectively statically loaded in precrushing operations to remove the high initial buckling load for the dynamic test.

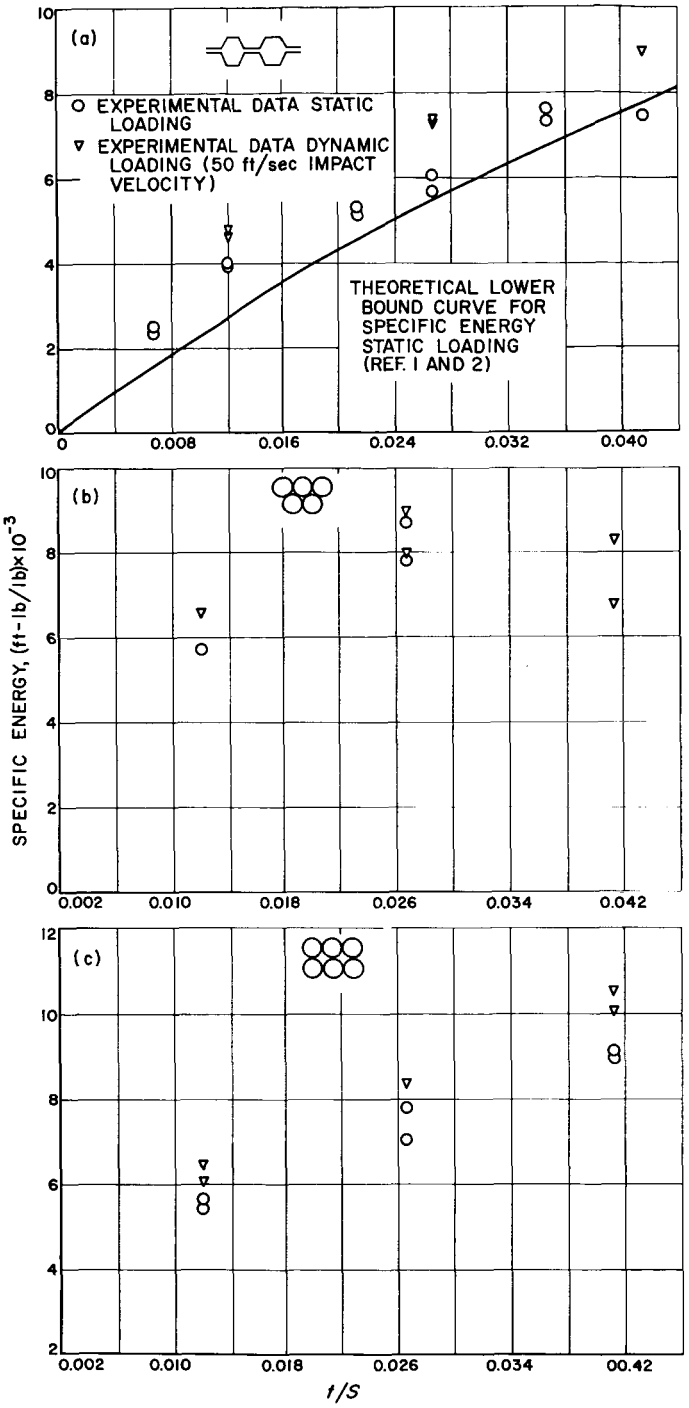

Fig. 35. Specific energy, 3003 H-19 aluminum

In an opposed sense, it was found that the static loading was a very severe test with regard to minor imperfections (such as dimples or buckles) in the honeycomb structure and particularly with regard to the propagation of these imperfections. Dynamic tests were satisfactorily performed on test specimens that had started severe progressive lateral failure modes under static loading.

Both results tend to strengthen the concept that the most appropriate way to test an energy-absorbing element is to subject it to a dynamic load.

B. Thickness Efficiency

As stated previously, one primary variable affecting the specific energy is the "thickness efficiency." At least one static test for each unit weight and cross-section considered in the testing program was continued until the specimen was fully crushed. The resulting thickness efficiencies are indicated in Figs. 36 through 38. For the hexagonal cell honeycomb, a least square best fit was determined from the data, assuming a linear relationship, and the standard deviation was determined as shown in Fig. 36. As shown, the thickness efficiency for the hexagonal cell honeycomb is a direct function of the honeycomb unit weight.

The data obtained for the tubular cell arrays are shown in Fig. 37; however, because of limited data points, only a trend can be established. A comparison of response for the three geometries is shown in Fig. 38.

It should be noted that, in an exact sense, these thickness efficiencies would quantitatively apply only to 3003 H-19 aluminum, since the ductility of the material would affect this relationship. Referring to Fig. 19, and noting the collapse mechanism, the effect of bend radius on thickness efficiency is apparent. The magnitude of variation in ductility from material to material would be

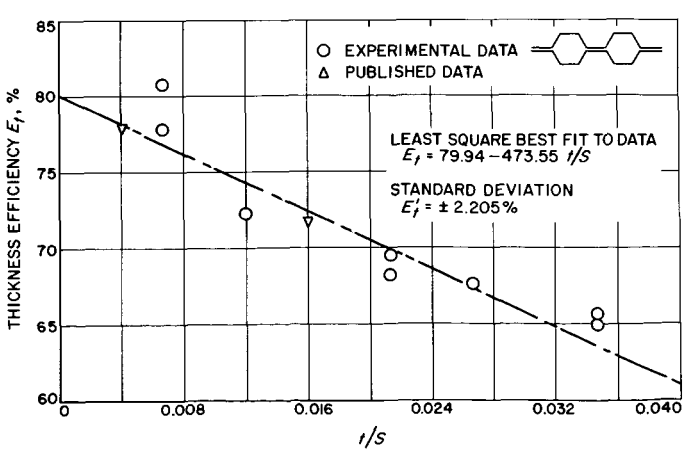

Fig. 36. Thickness efficiency, hexagonal cell honeycomb

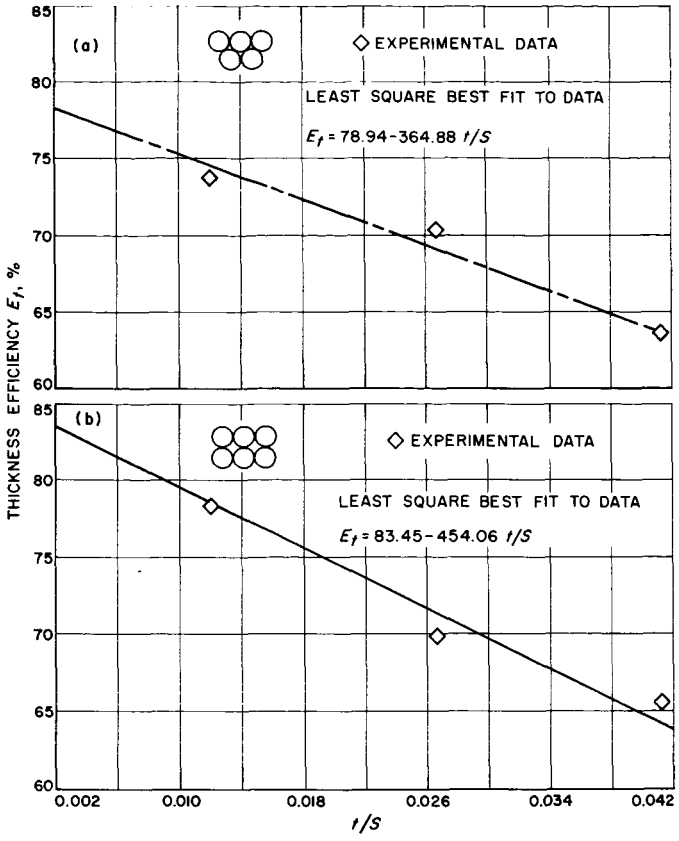

Fig. 37. Thickness efficiency, close-pack and loose-pack tubular cell honeycomb

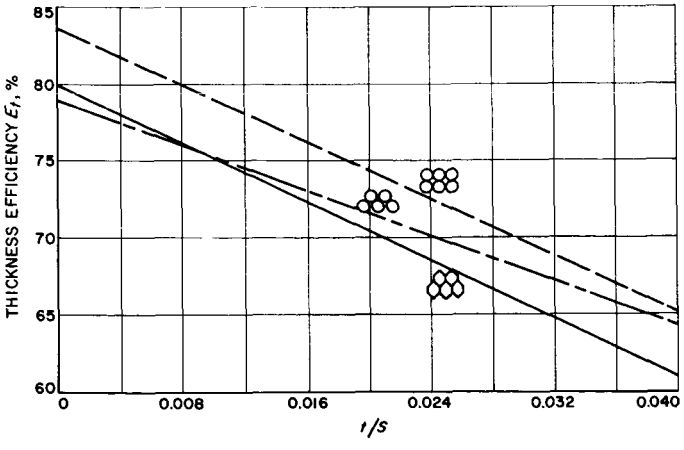

Fig. 38. Thickness efficiency

small, however, since a minimum ductility is required for the honeycomb to respond in the required collapse mode. Thus, qualitatively, we can say that the thickness efficiency is a direct function of the honeycomb unit weight, and for the aluminum hexagonal cell honeycomb it could vary from approximately 60 to 80%.

C. *Honeycomb Density*

The property of honeycomb whereby specific energy can be varied quantitatively by varying unit weight is a factor that has a large effect on the range of application and merit of honeycomb as an energy absorber. The limiting unit weight that proved feasible for energy absorption in terms of the cross-sectional geometry is a factor of prime interest in determining the most efficient cross section.

Referring to Fig. 35a, it is noted that there is a unit weight for the hexagonal cell honeycomb beyond which the slope of the specific energy curve decreases. Figure 20 shows that at this critical unit weight the mode of response that develops is essentially a shear mode, thus establishing an upper limit on the honeycomb unit weight. This response is primarily a characteristic of the honeycomb unit weight. However, loading rate and perhaps material properties could have an effect on the unit weight at which this mode appears. Also, if the height of the specimen was much less than the cross-sectional dimensions, this response mode could be restrained such that larger unit weights, yielding greater specific energies, could be used and this mode would not appear.

With the tubular cell honeycomb arrays, particularly the close-pack array, tests results show a very strong limiting unit weight. As shown in Fig. 35b, a limiting density occurs for static loading at a t/S ratio of approximately 0.032. There are no static loading test results for the close-pack array at the maximum unit weight since the specimens failed completely. The mode of failure is shown in Fig. 23. Figure 35b also shows a response of the close-pack array for a dynamic load. However, the specific energy for the maximum-unit-weight specimens is much lower than anticipated, indicating an unsatisfactory mode of response. This result would tend to indicate that the static load test would give conservative results with regard to limiting unit weights.

The loose-pack array responded as expected at the maximum unit weight tested, indicating an ability to collapse in the mode expected at honeycomb unit weights greater than the close-pack array. Considering maximum specific energy capabilities, the loose-pack array appears to offer the greatest efficiencies. Figure 25 illustrates a typical mode of response for this cross-sectional geometry at the maximum honeycomb unit weight tested.

An additional effect that honeycomb unit weight has on the hexagonal cell honeycomb response is apparent in the variation of load during the crushing or collapsing

process. As shown in Fig. 6, at the low honeycomb unit weights ($t/S = 0.0067$) there is a large variation of load during crushing (approximately $\pm 10\%$), but as the density increases the variation of load proportionately decreases, until at a t/S ratio of approximately 0.025 the variation stabilizes out to ± 2.5 to 3.0% and maintains this variation for increases in unit weight. This phenomenon does not occur in the tubular cell honeycomb.

The acceleration–time traces in Figs. 9 through 17 offer a better indication of specimen response than do the static loading curves. Particularly, looking at Figs. 12, 13, and 14 in sequence indicates a deterioration of the mode of response which is strongly shown in Fig. 14. Similarly, looking at Figs. 15, 16, and 17 in sequence would indicate that the mode of response in Fig. 17 was approaching a point of deterioration. Thus the acceleration–time traces provide a means of very effectively determining the limiting maximum honeycomb unit weight.

D. Maraging Steel Honeycomb

Considering the relationship previously stated for determining the specific energy of a metal honeycomb and utilizing concepts developed in Ref. 1, we may state,

$$Specific\ Energy = (Constant)\ \frac{\sigma_{yp}}{\gamma}$$

for a particular honeycomb unit weight. Thus, to increase the specific energy, we would seek a material with a greater yield-strength-to-material-density ratio capable of deforming in the mode of collapse associated with metal honeycomb. Following this criterion, the maraging steel was utilized to fabricate the test specimens as previously described.

A point of primary consideration in performing the static tests on the maraging steel specimens was the ability to correlate test data with computed data using relationships developed in Ref. 1. In this paper a relationship was generated to compute the mean crushing stress of metal honeycomb, assuming a rigid plastic response:

$$P_{(psi)} = \sigma_{yp} \frac{t^2}{S^2}\left[\frac{4.750}{K} + 28.628\right] + 1.155\, g_{yp}\, t/S \qquad (1)$$

The rigid plastic response assumes a relation between the plastic moment and yield stress as:

$$M_{yp} = 0.25\, t^2\, \sigma_{yp}$$

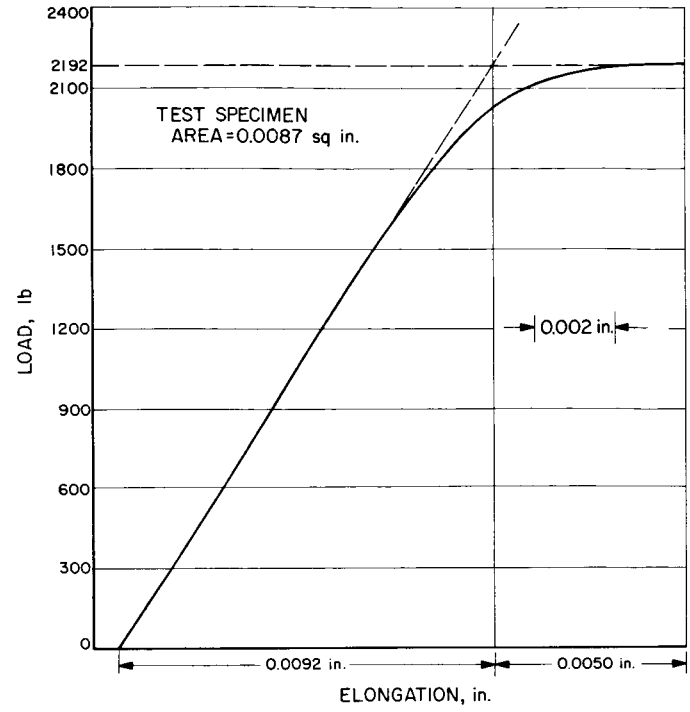

Fig. 39. Load elongation curve, maraging steel

For an elastic-plastic response, we would obtain the same relationship, but with a constant less than 0.25. Referring to Fig. 39, which is a load-elongation curve for the maraging steel, we can readily idealize this curve to an elastic-plastic response, with little error involved.

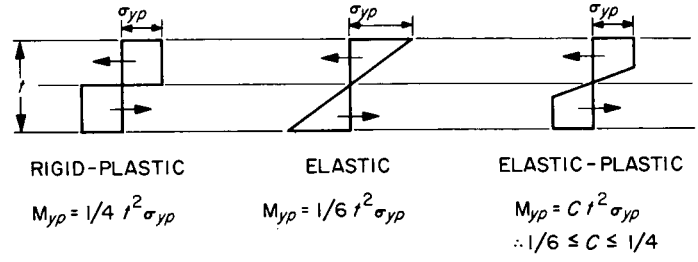

Referring to the above illustration, Eq. (1) can be rewritten to incorporate the factor C, which represents degree of plastic response. Thus:

$$P = \sigma_{yp}\, C\, \frac{t^2}{S^2}\left[\frac{19.002}{K} + 114.509\right] + 1.155\, g_{yp}\, t/S \qquad (2)$$

or letting $K = 0.40$ as stated in Ref. 1,

$$P = \sigma_{yp}\, C\, \frac{t^2}{S^2}[162.014] + 1.155\, g_{yp}\, t/S \qquad (3)$$

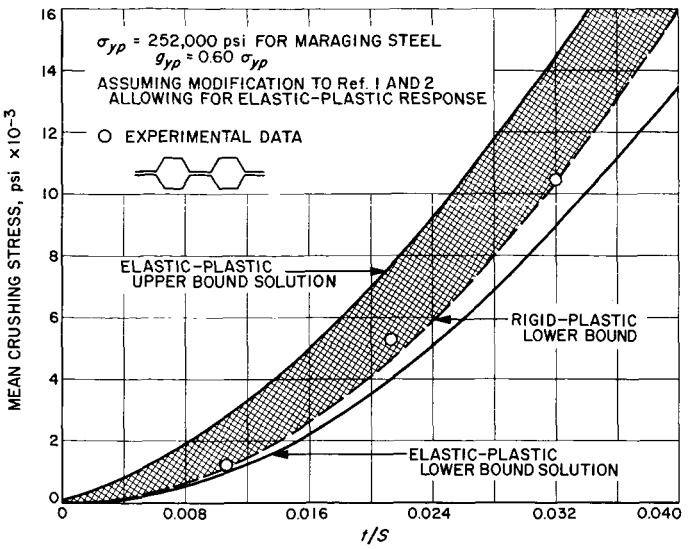

Fig. 40. Mean crushing stress, maraging steel hexagonal cell honeycomb, static loading

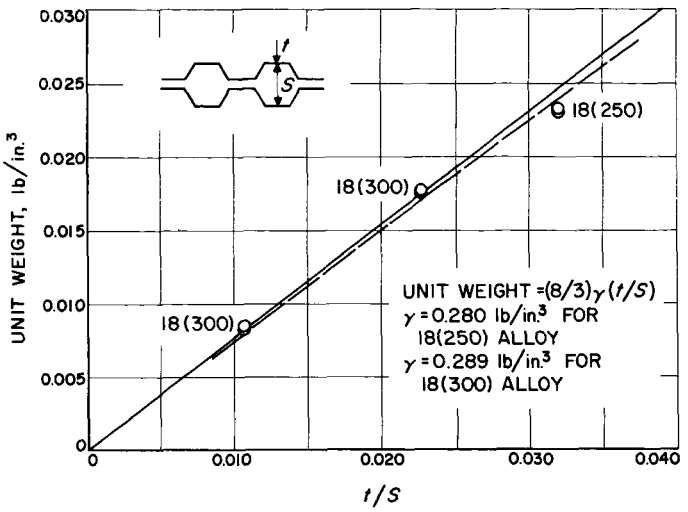

Fig. 41. Unit weight of maraging steel hexagonal cell honeycomb

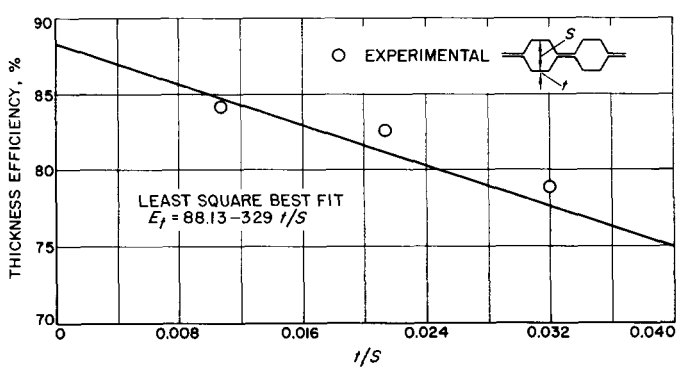

Fig. 42. Thickness efficiency, maraging steel hexagonal cell honeycomb

Computing C, with the use of Fig. 39, we obtain $C = 0.215$. Therefore:

$$P = \sigma_{yp}\frac{t^2}{S^2}\,[34.83] + 1.155\, g_{yp}\, t/S \qquad (4)$$

Plotting the first term of this expression will give the lower-bound crushing stress of maraging steel honeycomb, and the entire expression will indicate an upper bound on the crushing stress, as indicated in Fig. 40.

The upper- and lower-bound solution is a characteristic of the analytical technique used, and essentially indicates that, if the honeycomb collapses in the crushing mode assumed, then the mean crushing stress will always fall between these calculated bounds. Referring again to Fig. 40, it is noted that the bounded region is quite large and that the upper bound has little meaning. Test data for the maraging steel are shown in Fig. 40, and, as with the aluminum honeycomb, the lower-bound solution closely and conservatively approximates the response of the honeycomb.

Figure 41 indicates the unit weights of the maraging steel specimens; Fig. 42 indicates the thickness efficiencies obtained experimentally.

Utilizing the lower-bound elastic-plastic solution, which is the first term only of Eq. (4), plus the unit-weight and thickness-efficiency relationships indicated in Figs. 41 and 42, we can readily compute a lower-bound curve for the specific energy of maraging steel hexagonal cell honeycomb (see Fig. 43).

This computed result would, of necessity, indicate conservative values and would never exceed actual measured values for the typical honeycomb mode of response. As shown by Fig. 43, the original rigid-plastic assumption would provide results more consistent with present experimental data; however, this could be a characteristic of the maraging steel. Assuming that this lower-bound elastic-plastic solution is not excessively conservative, we can then state that, with maraging-steel hexagonal cell honeycomb subjected to static loading, the maximum specific energy that could be obtained is "at least" 28,500 ft-lb/lb. If we were to apply the rigid-plastic assumption, the maximum specific energy that could be obtained from maraging-steel hexagonal cell honeycomb, statically

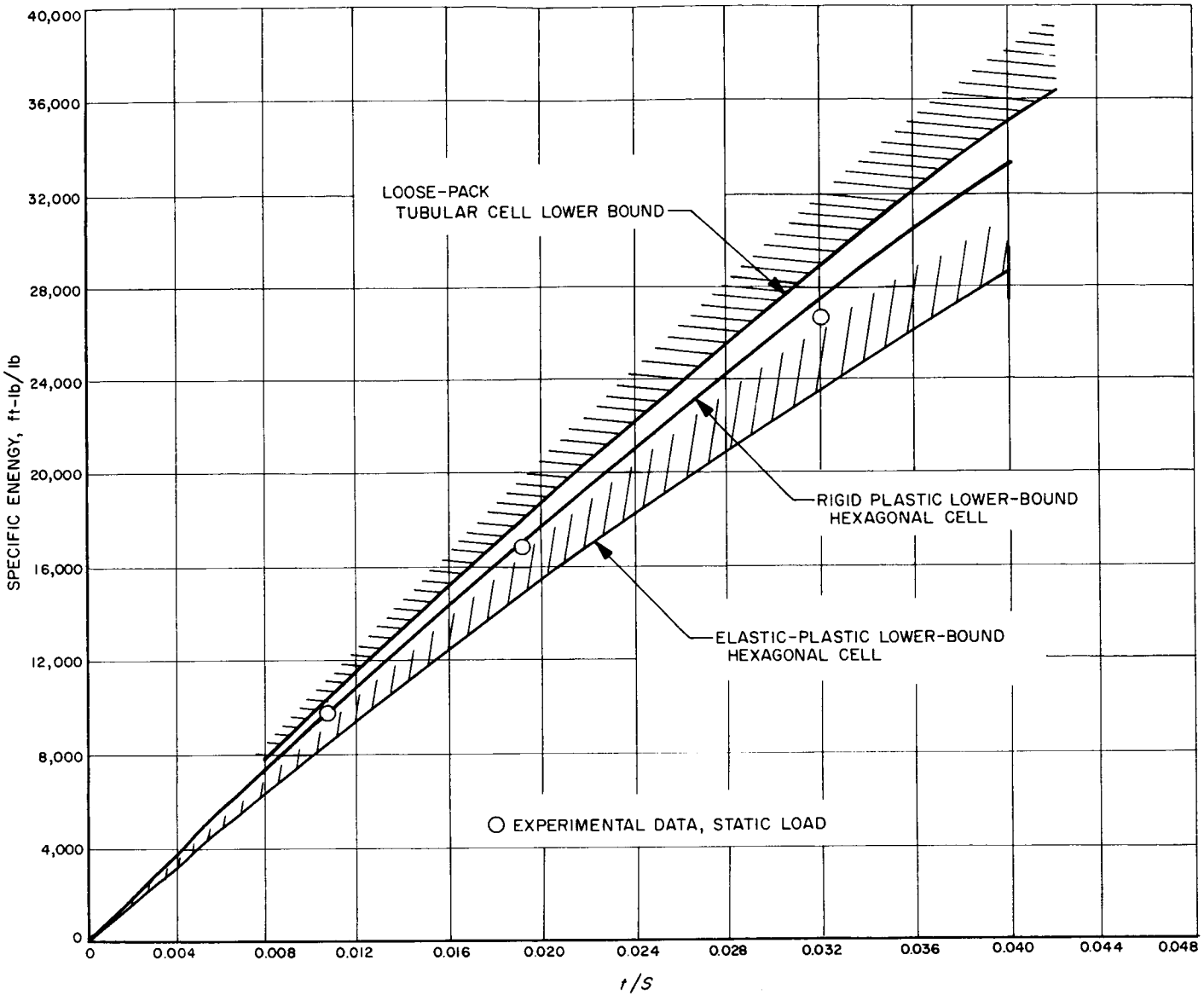

Fig. 43. Specific energy, maraging steel honeycomb

loaded, would be "approximately" 33,000 ft-lb/lb. From Figs. 31, 32, and 33 it is apparent that the maraging steel does not have adequate ductility to fully collapse, but appears to frange slightly during the final stages of collapse. It is this factor that allows for the very high thickness efficiency, as indicated by Fig. 42, and contributes to the very small rebound. The maraging steel is well suited to this application, as indicated by the specific energy values, and due to the limited franging characteristics and it is likely that maximum honeycomb densities greater than the limiting value established for aluminum could be obtained.

V. CONCLUSIONS

The end result of this development program was essentially a qualitative one, that of determining the relative importance and range of the variables that affect the energy-absorbing characteristics of axially loaded metal honeycomb. The results can be summarized as follows:

1. The specific energy of metal hexagonal cell honeycomb, subjected to axial static loading, can be computed provided thickness efficiency, as a function of honeycomb unit weight, is known. In addition, for a given material yield stress, or a representation of the equivalent elastic–plastic yield moment, the maximum specific energy can be determined.
2. The specific energy can be closely approximated for the tubular cell honeycomb by utilizing computed data for hexagonal cell honeycomb. Utilizing the loose-pack tubular cell geometry, the maximum specific energy for a given material can be approximated, giving the largest specific energy values possible when using a honeycomb array to absorb kinetic energy.
3. When the impact velocity is no greater than 50 ft/sec, the effect of dynamic loading is essentially the same as static loading for metal honeycomb when loading axially.

Additional work is needed in order to completely evaluate honeycomb as an energy absorber. In particular, the two primary areas that remain to be evaluated are (1) the effect of velocity of impact on the specific energy for velocities in excess of 50 ft/sec, and (2) the effect of nonaxial loading on the specific energy. This latter topic is considered to a limited extent for commercial honeycomb in Ref. No. 3.

REFERENCES

1. McFarland, R. K., *A Limit Analysis of Energy Absorbing Structural Elements*, Technical Report 32-186, Jet Propulsion Laboratory, Pasadena, Calif., December 1961.
2. McFarland, R. K., "Hexagonal Cell Structures Under Post-Buckling Axial Load," *AIAA Journal*, Vol. 1, June 1963.
3. Flora, C. L., *Impact Deceleration Systems Applicable to Lunar Landing Vehicles*, Report 2324, Radioplane, Div. of Northrop Corp., Van Nuys, Calif., November 21, 1960.

BIBLIOGRAPHY

1. Ali, A., and Benson, L. R., *Cushioning for Air Drop. Part IX, Bibliography of Literature Pertaining to the Absorption of Impact Energy,* Report DA-19-129-QM-150, Structural Mechanics Research Laboratory, University of Texas, Austin, Texas, June 9, 1957.

2. Ali, A., et al., *Cushioning for Air Drop. Part VI, Preliminary Investigation of the Absorption of Shock Energy by Wood in Lateral Compression,* Report DA-19-129-QM-150, Structural Mechanics Research Laboratory, University of Texas, Austin, Texas, March 18, 1957.

3. Ali, A., *Cushioning for Air Drop. Part VIII, Dynamic Stress-Strain Characteristics of Various Materials,* Report DA-19-129-QM-150, Structural Mechanics Research Laboratory, University of Texas, Austin, Texas, June 3, 1957.

4. Anderson, Roger A., "Research, Design Considerations, and Technological Problems of Structures for Planetary Entry Vehicles," *Proceedings of the NASA–University Conference on the Science and Technology of Space Exploration,* Vol. 2, NASA SP-11 Washington, D.C., December 1962.

5. Bixby, H. W., *Impact Attenuation Methods for Manned Spacecraft,* TR 63, Northrop Corporation, Ventura, Calif.

6. Bixby, H. W., *Development of a Paperboard Honeycomb Decelerator for Use with Large Platforms in Aerial Delivery Systems,* WADC TR 59-776, Wright Air Development Center, Wright-Patterson AFB, Ohio, 1959.

7. Blanchard, V. J., *Landing-Impact Characteristics of Load Alleviating Struts on a Model of a Winged Space Vehicle,* NASA TN D-541, Washington, D.C., 1960.

8. Burns, Andrew B., and Pascyk, James A., *Lunar Alightment Systems Investigation* (February 1962–May 1963) Report AF33(657)-8197, American Machine and Foundry Co., Aeronautical Systems Division, Wright-Patterson AFB, Ohio, 1963.

9. *Characteristics of Energy Absorbing Materials for a Lunar Soft Landing Vehicle,* 9753-0001-MU-000, Space Technology Laboratories, Los Angeles, Calif., 1961.

10. *Concepts of Multiple-Impact Study of Energy Absorption,* Quarterly Progress Reports to NASA (under Contract NAS 7-226), Aerospace Research Associates, Inc., West Covina, Calif., 1963.

11. Collins, F. L., *Physical Characteristics of Cushioning Materials. III, Energy Absorption Characteristics,* Chemical Inspectorate, Memo 47 (ASTIA AD-5799), Great Britain, November 1952.

12. Coppa, A. P., *Buckling of Circular Cylindrical Shells Subject to Axial Impact,* NASA TN D-1510, Washington, D.C., 1962.

13. Coppa, A. P., *Collapsible Shell Structures for Lunar Landings,* T.I.S. Report R 62 SD9, General Electric Co., Schenectady, N.Y., 1962.

14. Daigle, D., and Lonborg, J. O., *Evaluation of Certain Crushable Materials,* Technical Report 32-120, Jet Propulsion Laboratory, Pasadena, Calif., January 13, 1961.

BIBLOGRAPHY (Cont'd)

15. Dye, E. F., "Impact Protection with Foam Plastics," *Mechanical Engineering,* Vol. 80, December 1958, p. 65.

16. *Energy Absorption of Aluminum Honeycomb,* No. TSB-110, Hexcel Products, Inc., Berkeley, Calif., January 1960.

17. "Energy Absorbing Systems," *Research Summary No. 36-5,* Vol. I, Jet Propulsion Laboratory, Pasadena, Calif., October 15, 1960.

18. Esgar, Jack B., *Survey of Energy-Absorption Devices for Soft Landing of Space Vehicles,* NASA TN D-1308, Washington, D.C., 1962.

19. Fisher, Floyd J., Jr., *Landing-Impact Dissipation Systems,* NASA TN D-975, Washington, D.C., 1961.

20. Goldsmith, Werner, *Impact: the Theory and Behaviour of Colliding Solids,* Edwin Arnold, Ltd., London, 1960.

21. Karnes, Charles H., Turnbou, James W., et al, *High Velocity Impact Cushioning, Part V, Energy-Absorption Characteristics of Paper Honeycomb,* Structural Mechanics Research Laboratory, University of Texas, Austin, Texas, March 25, 1959.

22. Kornhauser, M., *Structural Effects of Impact,* Spartan Books, Inc., Baltimore, Md., 1964.

23. *Landing Shock Absorption,* MU60-389, Space and Information Systems Division, North American Aviation, Inc., Downey, Calif.

24. Lewallen, J. M., *Energy-Dissipating Characteristics of Trussgrid Aluminum Honeycomb,* SMRL-RM-5, University of Texas, Austin, Texas, March 1962.

25. McFarland, R. K., "Development of Energy Absorbing Structural Elements," *Space Programs Summary No. 37-18, Vol. IV,* Jet Propulsion Laboratory, Pasadena, Calif., December 1962.

26. McFarland, R .K., "Development of Energy Absorbing Systems," *Space Programs Summary No. 37-18, Vol. IV,* Jet Propulsion Laboratory, Pasadena, Calif., December 1962.

27. McGehee, John R., *A Preliminary Experimental Investigation of an Energy Absorption Process Employing Frangible Metal Tubing,* NASA TN D-1477, Washington, D.C., 1962.

28. Morgan, Carl W., and Moore, Walter L., *Cushioning for Air Drop. Part V, Theoretical and Experimental Investigations of Fluid-filled Metal Cylinders for Use as Energy Absorbers on Impact,* Report DA-19-129-QM-150, Structural Mechanics Research Laboratory, University of Texas, Austin, Texas, December 20, 1956.

29. O'Bryon, T. C., *Limited Investigation of Crushable Structures for Acceleration Protection of Occupants of Vehicles at Low Impact Speeds,* NASA TN D-58, Washington, D.C., October 1959.

30. *Performance Characteristics of Cushioning Material, Impact Under a Heavy Weight, High Impact Shock Machine,* TR 55-229, Wright Air Development Center, Dayton, Ohio, 1955.

BIBLIOGRAPHY (Cont'd)

31. "Properties of Foam and Laminates Under Shock Loading," Plas-Tech Equipment Corporation, *SPE Journal*, Vol. 15, January 1959.

32. *Properties and Uses of Balsa*, Balsa Ecuador Lumber Corp., 502 Fifth Ave., New York, N.Y.

33. *RF Transparent, Energy Absorbing, Structural Elements. Phase I, Final Report to JPL from General Electric*, G.E. Document 64 SD 565. Schenectady, N.Y., 1964.

34. Shield, R., and Corington, C., *High Velocity Impact Cushioning, Part VI. 108C and 100C Foamed Plastics*, Structural Mechanics Research Laboratory, University of Texas, Austin, Texas, September 1960.

35. Simonson, J. R., *A Study of Design Criteria for Landing Shock Absorption Devices for Recoverable Flight Vehicles*, ASD-TR-61-583, Aeronautical Systems Division, Wright-Patterson Air Force Base, Ohio, January 1962.

36. Turnbou, James W., et al, *Cushioning for Air Drop. Part III: Characteristics of Paper Honeycomb Under Dynamic Loading*, Report DA-19-129-QM-150, Structural Mechanics Research Laboratory, University of Texas, Austin, Texas, August 31, 1956.

37. Turnbou, James W., *Cushioning for Air Drop. Part VII, Characteristics of Foamed Plastics Under Dynamic Loading*, Report DA-19-129-QM-150, Structural Mechanics Research Laboratory, University of Texas, Austin, Texas, March 28, 1957.